National Library of Canada
Canadian Theses Service
Ottawa, Canada
K1A 0N4

Bibliothèque nationale du Canada
Services des thèses canadiennes

CANADIAN THESES

THÈSES CANADIENNES

NOTICE

The quality of this microfiche is heavily dependent upon the quality of the original thesis submitted for microfilming. Every effort has been made to ensure the highest quality of reproduction possible.

If pages are missing, contact the university which granted the degree.

Some pages may have indistinct print especially if the original pages were typed with a poor typewriter ribbon or if the university sent us an inferior photocopy.

Previously copyrighted materials (journal articles, published tests, etc.) are not filmed.

Reproduction in full or in part of this film is governed by the Canadian Copyright Act, R.S.C. 1970, c. C-30. Please read the authorization forms which accompany this thesis.

AVIS

La qualité de cette microfiche dépend grandement de la qualité de la thèse soumise au microfilmage. Nous avons tout fait pour assurer une qualité supérieure de reproduction.

S'il manque des pages, veuillez communiquer avec l'université qui a conféré le grade.

La qualité d'impression de certaines pages peut laisser à désirer, surtout si les pages originales ont été dactylographiées à l'aide d'un ruban usé ou si l'université nous a fait parvenir une photocopie de qualité inférieure.

Les documents qui font déjà l'objet d'un droit d'auteur (articles de revue, examens publiés, etc.) ne sont pas microfilmés.

La reproduction, même partielle, de ce microfilm est soumise à la Loi canadienne sur le droit d'auteur, SRC 1970, c. C-30. Veuillez prendre connaissance des formules d'autorisation qui accompagnent cette thèse.

THIS DISSERTATION
HAS BEEN MICROFILMED
EXACTLY AS RECEIVED

LA THÈSE A ÉTÉ
MICROFILMÉE TELLE QUE
NOUS L'AVONS REÇUE

NL 339 (r. 86/01)

Canada

0-315-24878-5

National Library of Canada
Canadian Theses Division
Ottawa, Canada
K1A 0N4

Bibliothèque nationale du Canada
Division des thèses canadiennes

PERMISSION TO MICROFILM — AUTORISATION DE MICROFILMER

• Please print or type — Écrire en lettres moulées ou dactylographier

Full Name of Author — Nom complet de l'auteur

Chul Hi Park

Date of Birth — Date de naissance

Jan. 22, 1960

Country of Birth — Lieu de naissance

Korea

Permanent Address — Résidence fixe

Nading Wonil Apt. #103
Dohadong 444-18
Inchon, Korea

Title of Thesis — Titre de la thèse

Multiple Scattering of Electrons Used in Medical Radiation Therapy

University — Université

University of Alberta

Degree for which thesis was presented — Grade pour lequel cette thèse fut présentée

M.Sc.

Year this degree conferred — Année d'obtention de ce grade

1984

Name of Supervisor — Nom du directeur de thèse

J. Scrimger & J. Battista

Permission is hereby granted to the NATIONAL LIBRARY OF CANADA to microfilm this thesis and to lend or sell copies of the film.

The author reserves other publication rights, and neither the thesis nor extensive extracts from it may be printed or otherwise reproduced without the author's written permission.

L'autorisation est, par la présente, accordée à la BIBLIOTHÈQUE NATIONALE DU CANADA de microfilmer cette thèse et de prêter ou de vendre des exemplaires du film.

L'auteur se réserve les autres droits de publication; ni la thèse ni de longs extraits de celle-ci ne doivent être imprimés ou autrement reproduits sans l'autorisation écrite de l'auteur.

Date

June 22, 1984

Signature

Chul Hi Park

NL-91 (4/77)

THE UNIVERSITY OF ALBERTA

MULTIPLE SCATTERING OF ELECTRONS USED IN MEDICAL RADIATION THERAPY

by

CHUL HI PARK

A THESIS

SUBMITTED TO THE FACULTY OF GRADUATE STUDIES AND RESEARCH

IN PARTIAL FULFILMENT OF THE REQUIREMENTS FOR THE DEGREE

OF MASTER OF SCIENCE

DEPARTMENT OF PHYSICS

EDMONTON, ALBERTA

FALL 1984

THE UNIVERSITY OF ALBERTA

RELEASE FORM

NAME OF AUTHOR CHUL HI PARK

TITLE OF THESIS MULTIPLE SCATTERING OF ELECTRONS USED IN MEDICAL RADIATION THERAPY

DEGREE FOR WHICH THESES WAS PRESENTED MASTER OF SCIENCE

YEAR THIS DEGREE GRANTED 1984

Permission is hereby granted to THE UNIVERSITY OF ALBERTA LIBRARY to produce single copies of this thesis and to lend or sell such copies for private, scholarly scientific research purposes only.

The author reserves other publication rights, and neither the thesis nor extensive extracts from it may be printed or otherwise reproduced without the author's written permission.

Chul Hi Park

PERMANENT ADDRESS:

NADONG WONIL APT. #103

DOHADONG 444-18

INCHON 160

KOREA

DATED May 1 1984

THE UNIVERSITY OF ALBERTA

FACULTY OF GRADUATE STUDIES AND RESEARCH

The undersined certify they have read, and recommend to the Faculty of Graduate Studies and Research, for acceptence, a thesis entitled

MULTIPLE SCATTERING OF ELECTRONS USED IN MEDICAL RADIATION THERAPY

submitted by Chul Hi Park

in partial fulfilment of the requirements for the degree of Master of Science

J. Battiste

J. W. Scrimger

.....

Supervisor

Cameron J. Kost

.....

S. Rathbun

.....

Anton F. Leyton

.....

Date: June 20, 1984

to my parents

ABSTRACT

Since the initiation of electron radiation therapy, most of the experimental efforts to understand the transport of electrons in a medium have been concentrated on the investigation of dose deposition by electrons. Because the dose distribution of an electron beam is only the end result of the transport of electrons, it has not been possible to predict the dose distribution in a complex medium. In addition, the prediction of a dose distribution even for a simple medium, such as, an all water "phantom", cannot be made generally because of the the degradation of the accelerated beam caused by the method of shaping a broad beam(e.g., scattering foil and collimator).

In this study of electron transport in a homogeneous semi-infinite medium, the linearized Boltzmann transport equation is used with the boundary condition of an individual pencil beam is used. To facilitate the mathematical treatment of the problem, the medium is divided into two regions. The first region is where the path-length of an electron is still far shorter than the "diffusion length" of the medium. By applying the "Fokker-Plank" approximation we obtain the angular distribution of electrons and the average lateral, and longitudinal displacements. The second region is where the orientations of electrons has become very diffuse. In

order to take care of the energy dependence of the scattering cross-section, we use the "continuous slowing down approximation". The angular density function is expanded in terms of spherical harmonics and the scattering cross-section is also expanded by the Legendre polynomial. The series is truncated at m=1 and n=1. The spatial distribution of electrons is obtained by solving the resulting coupled equations.

Results are compared to those obtained by Fermi and discrepancies are found in angular distributions of electrons. Furthermore, it is pointed out that Fermi's solution has a serious drawback because the depth of the medium is used as an energy indicator instead of the actual path-length of eletrons. Its application to the radiation transport problem is thus inappropriate, despite its popularity in applications to medical physics problems.

ACKNOWLEDGMENTS

I wish to thank my supervisors Drs. J. Battista and J. Scrimger for their constant encouragement and outstanding guidance throughout the course of this work.

I would like to express my special gratitude to Dr. S. Usiskin and Mr. R. Mackie for their constant support and encouragement in adjusting to a new way of life. Without them, even this megre result could not have been achieved.

I would also like to thank all the colleagues in the Medical Physics Department of Cross Cancer Institute for helping me out in various ways during this study.

Finally, I greatly appreciate the financial assistance of the Department of Physics, the Alberta Cancer Board, and the Alberta Heritage Foundation for Medical Research.

TABLE OF CONTENTS

CHAPTER I INTRODUCTION

I.1 History of Radiation Therapy with Electrons . . . 1

I.2 Physical Description of Broad Electron Beams . . . 5

I.2.1 Beam Energy 5

I.2.2 Energy Spectrum 11

I.2.3 Field Size 11

I.2.4 Field Uniformity And Symmetry 12

I.2.5 Mass Stopping Power 15

I.2.6 Mass Angular Scattering Power 16

I.3 Electron Beam Treatment Planning 17

I.3.1 Description of The Patient 17

I.3.2 Dose Distribution 18

I.3.3 Characteristics of Depth Dose Curves 23

I.3.4 Field Shaping 23

I.3.5 Isodose Curves 23

I.3.6 Interactions in Heterogeneous Tissue 24

I.4 Present Theoretical Model for Electron Transport . 27

CHAPTER II REVIEW OF DOSE CALCULATION METHODS

II.1 Absorption Equivalent Thickness Method 30

II.2 Coefficient of Equivalent Thickness (CET) Method . 34

II.3 Modified Absorption Coefficient (MAC) Method . . . 37

II.4 Correction Method for Edge Effects 39

II.5 Approximation of Isodose Curves by the Age

Diffusion Solution 42
II.6 Pencil Beam Analysis of Broad Beam 44
II.7 Summary 46

CHAPTER III TRANSPORT OF ELECTRONS IN A SCATTERING MEDIUM
III.1 Introduction 50
III.2 Some Aspects of Electron Transport in a Scattering Medium 51
III.3 Multiple Scattering and the Linearized Boltzmann Equation 52
III.3.1 Fokker-Plank Approximation At Shallow Depth . 54
III.3.2 Applications to the Shallow Depth Problem . . 62
III.3.3 Diffusion In Deeper Regions 68
III.4 Discussion 75

CHAPTER IV CONCLUSION AND FUTURE WORK 80

REFERENCES 84
APPENDIX A RELATIONSHIP OF BOLTZMANN AND FERMI EQUATIONS 89

LIST OF FIGURES

Figure		Page
1.	Depth dose curves of broad beams of electrons of various energies incident on a water phantom	3
2.	Typical treatment head of medical accelerator used for electron radiation therapy	7
3.	Definition of various energies used in electron radiation therapy	9
4.	The effect of tilted surface of a medium on the dose distribution	21
5.	Constriction of the 80% and 90% isodose lines in comparison with the geometric field size (at surface)	25
6.	Central axis depth dose distribution produced in high-impact polystyrene and 2.0 cm high-impact polystyrene followed by cork, by electron beams of indicated energies	31
7.	Calculation of isodose distribution with correction for bone and lung inhomogeneity	33
8.	Coordinates and parameters used for the calculation of CET and MAT methods	35
9.	Energy dependence of the angles ans	
10.	Maximum changes in absorbed dose behind edges	40
11.	Measured dose distribution behind a lead strip	

in a water 41

12. Calculated isodose distributions in water, assuming a monoenergetic incident electron energy of 15 MeV and a field size of 10 cm with a parallel beam 43

13. Schematic representation in the X-Z plane of a therapeutic electron beam incident on a patient 45

14. The plot of the angular distribution function $f(\Theta,\ell)$ for various ℓ . 76

15. The angular distribution function of electrons 76

CHAPTER I

INTRODUCTION

I.1 History of Radiation Therapy with Electrons

In 1934, Brasch and Lange(1) reported on the use of "fast cathode rays" as a method of radiation therapy. This is apparently the first paper dealing with the use of external beams of electrons as a therapeutic agent. They cited as advantages;

(a) well defined and adjustable range of penetration;

(b) ability to deliver more dose at depth relative to the dose at surface ("skin sparing");

(c) enhanced biological response; and

(d) the possibility of magnetic directability.

The energy of the electrons they used was between 0.7 MeV and 2 MeV, with a range of up to approximately 1 cm in soft

tissue. The first mention of the use of higher energy electron beams was made by Hass et al.(2) in 1954. These authors pointed out the advantages described previously and also stated that the skin reaction was not worse than that experienced with other types of radiation. This paper dealt with electron beams produced with a 22 MeV betatron.

Electron radiation therapy was initiated mainly because of the advantageous penetration characteristics(a and b) and it evolved rapidly with the development of reliable higher energy accelerators. The early method of dose administration was based largely on the energy deposition data measured in a homogeneous medium, such as a water "phantom"(Figure 1). This approach is based on the assumption that the volume of the patient's body to be irradiated is of unit density and water-like in atomic composition. The dose distribution of an electron beam is assumed not to be severely distorted as it penetrates heterogeneous tissue. This dose administration method is therefore based on the simple consideration of the cross-sectional area and the depth of the tumor from the skin surface, which determine the field size and beam energy, respectively.

In 1961, Ovadia and McAllister(3) reported improved "skin sparing" and the reduction of dose to normal tissue overlying tumors with the use of a "grid" placed in the

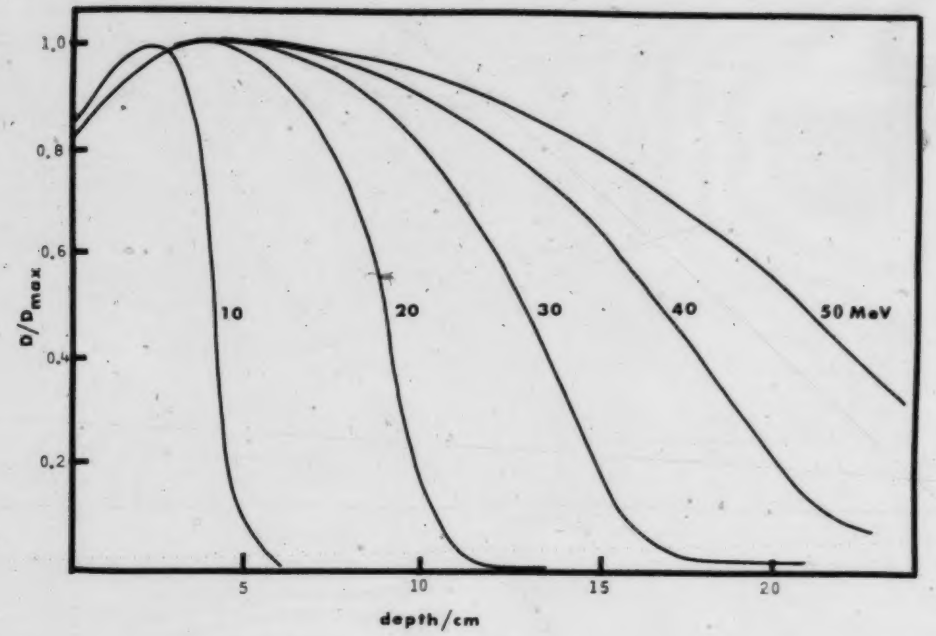

Fig. 1. Depth dose curves of broad beam of electrons of various energies incident on a water phantom

incident beam. The grid was constructed of a lead mask(1.25 cm thick) with holes of various size. These authors optimized the hole size and spacing to achieve dose reduction in the skin and "transit" tissue. In 1963, there was another report of a similar effect without the use of a grid by Carpender et al.(4) who described electron radiation therapy with a scanned "pencil beam". This concept of a "pencil beam" is important and will be emphasized in this thesis. They found less skin reactions, and gave several explanations;

(a) "grid-effect" caused by the raster scan pattern,

(b) higher local dose rate,

(c) uncontaminated beam of electrons achieved by not using a scattering foil to produce a macroscopic beam by spreading a pencil beam.

However, they were doubtful about the first explanation, because the scanning was performed continuously to give a homogeneous surface dose. Furthermore, daily variations in positioning of the field on the patient would further diffuse or blurr the raster pattern.

Another significant finding was the actual alteration of the depth dose curve(Figure 1), caused by tissue inhomogeneity. Taply and Fletcher(5) summarized various clinical complications caused by overdosage due to

the presence of lung in 1964. Several years before this, simple corrections(i.e., CET) for tissue inhomogeneity had been developed by Laughlin.(6) Basically, this method relies upon the modification of standard central axis dose data on the basis of the average density of tissue actually traversed. At that time, the lack of information of the anatomy of the patient presented an unsolved problem and more complex schemes which consider electron transport were not developed. With the advent of X-ray computed tomography which provides not only the geometry of the patient's anatomy but also an in vivo map of tissue densities, one of the fundamental obstacles to accurate treatment planning was removed.(9,11,12) However, in spite of this remarkable progress in obtaining patient-specific data, the complexity of electron transport in a heterogeneous medium has yet to be fully understood and this remains as a problem today.

I.2 Physical Description of Broad Electron Beams

I.2.1 Beam Energy

The energy is perhaps the most important parameter in that it is directly related to the location of abrupt fall-off in the depth dose curve, as measured in a

homogeneous medium. Selection of an appropriate energy permits the treatment of a lesion located near a surface and extending to a specified depth (e.g. chest wall). In fact this trend of depth dose curves to fall off sharply has been used reciprocally to define the "mean energy" of a broad beam of electrons.

The nominal energy of electrons is fixed and uniquely defined by the accelerating potential. Even though there is a small spread in energy(<1%) within the accelerator, we can characterize this energy by a monoenergetic value E_a , the "accelerator energy". The accelerated narrow beam of electrons, however, has to pass through exit windows of the accelerator space, scattering foils, mirrors, dose monitor chambers, and air layers of considerable total thickness before reaching the body surface.(Figure 2) A cascade of energy losses in these materials shifts the electron energy to less than E_a , and also broaden the spectrum as a result of fluctuations in energy loss. Provided these fluctuations in energy loss are very small, one can still speak of a single energy value, E_0 , at the body surface;

$$E_0 = E_a - \Delta E_{tot}$$

where ΔE_{tot} is the total mean energy loss in the layers traversed by the beam before reaching the patient. In a

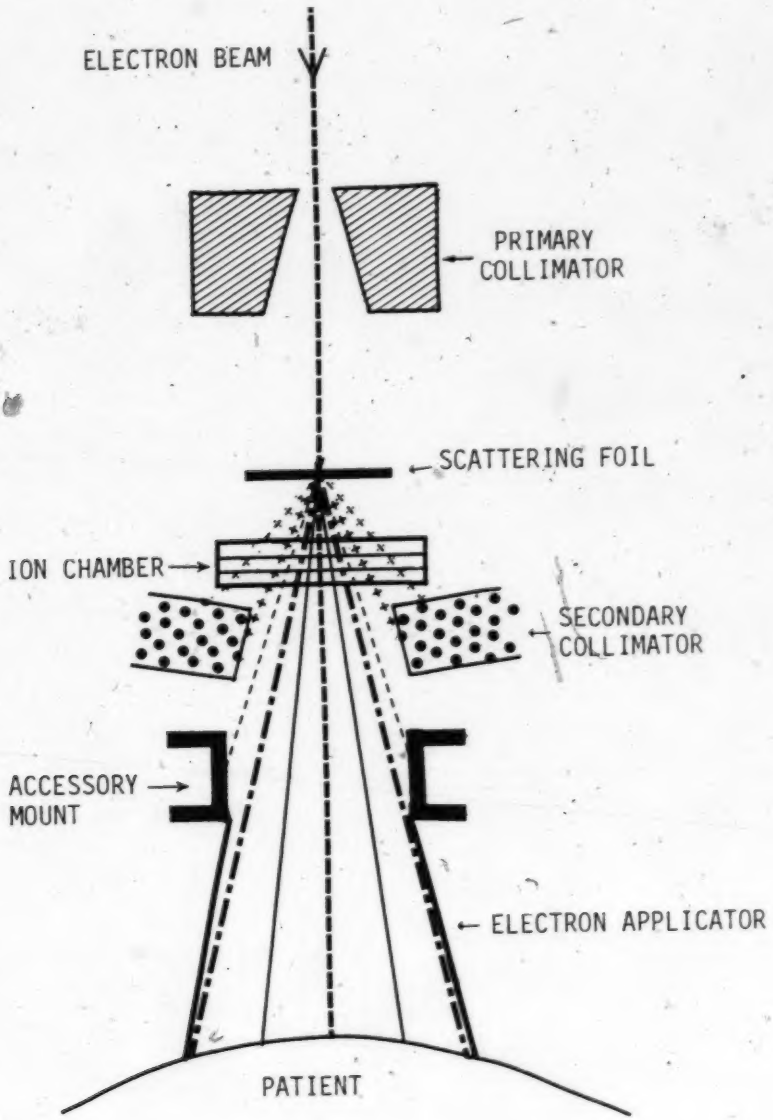

Fig. 2. Typical treatment head of medical accelerator used for electron radiation therapy

practical situation, this quantity is difficult to calculate, although a measurement is possible(49). Beyond layers of the tissues of appreciable thickness in an irradiated body, one has to consider a further distribution of the electron fluence in energy, which is influenced by the incident spectrum, further energy losses in penetrating into the body, and the generation of secondary electrons. The distribution may be characterized by the most probable energy, the mean energy, and the maximum energy at a particular site in the body.

According to the ICRU(17), there are four possible statements of energy currently in use;

(a) E_a , with description of the scattering foils(if any);

(b) the "most probable energy" at the surface of the body ;

(c) the "mean energy" at the surface of the body ;

(d) energies determined experimentally using various methods that yield values of one of the above three energies. These quantities are shown in Figure 3.

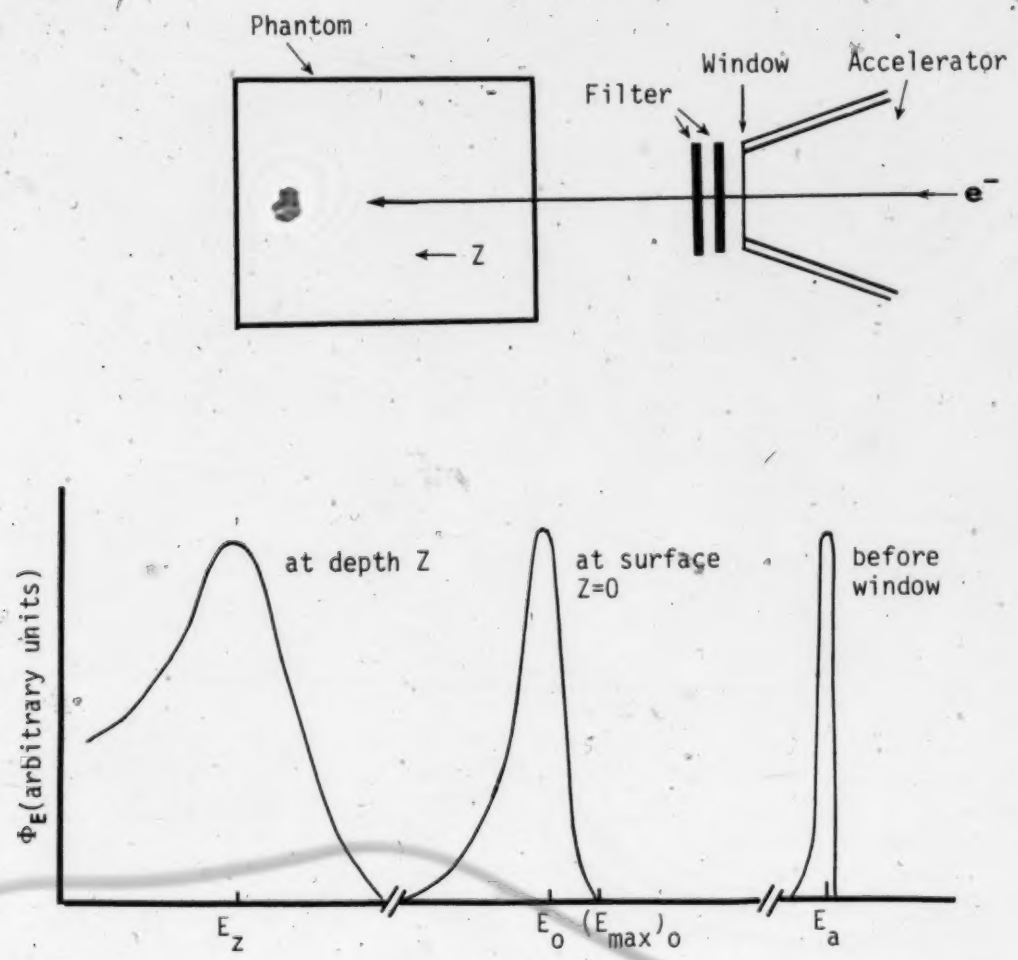

Fig. 3. Definition of various energies used in electron radiation therapy. Φ_E is the distribution of fluence in energy. (17)

E_a: The accelerator energy
E_{max}: The maximum energy at the surface
E_0: The energy at the surface of medium
E_z: The energy at depth Z

I.2.2 Energy Spectrum

The quality of the electron beam is characterized fully by its energy spectrum, $\bar{E}$ (assuming no photon contaminations). The energy spectrum determines the yields of energy-dependent physical, chemical, and biological effects. The energy spectrum also has a considerable clinical significance because it influences the actual dose distribution of electron beams (e.g. sharpness of the dose fall-off region). Moreover, the stopping power of the medium, which is energy-dependent, is the basis of the calculation of the absorbed dose. In defining the spectrum, the interesting quantity is the particle fluence, that is, the number of electrons passing through a unit area, per unit time, per unit energy(17). Experimental information about the fluence within an irradiated medium, is very hard to obtain, often one must rely on calculation.(18,19)

Another important quantity related to energy spectra of electrons is the distribution of electrons per unit solid angle for a particular direction of motion. This quantity is essential information for understanding influence of tissue inhomogeneity on electron dose distributions. Multiple scattering of electrons in a complex medium poses tremendous difficulties in calculating or measuring this fundamental quantity.

I.2.3 Field Size

Because of clinical requirements, the field size of the external electron beam must be variable. As part of the specification of the electron beam, the field has to have a shape and size compatible with the spatial distribution of the tumor and surrounding healthy tissue. Generally, rectangular fields are produced by the collimators in the treatment head(Figure 2), but these can be shaped further with secondary block to produce irregularly-shaped fields.

I.2.4 Field Uniformity And Symmetry

Field uniformity and symmetry are specified at a fixed depth in a homogeneous phantom for a portion of the geometric field area at that depth. The reference depth is often taken as the depth along the central axis at which 90% of the maximum dose is delivered. However, if we are truly interested in understanding field uniformity and symmetry, we should also consider the electron fluence(the number of electrons per unit solid angle for a specific direction of motion, per unit energy, per unit volume). The absorbed dose is only the end product of interactions between the electrons and the constituent atoms of the medium. A uniform absorbed dose distribution over the

field can be formed by many different fluence distributions, which are more of fundamental importance.

I.2.5 Mass Stopping Power

An understanding of the interaction of charged particles with matter is important, because the detection and influence of all types of radiation on all subtances, living or not, is through this interaction. For example, the detection of neutral particles(e.g. neutrons, photons) can only take place indirectly, i.e., after these have produced secondary charged particles(e.g., electron, proton) which dissipate enough energy to be detectable. Because several processes contribute to the slowing down of a fast charged particle, it is convenient to discuss stopping power in three different energy intervals;

(a) low energy, below approximately $10^{-4}mc^2$ (m is mass of electron)

(b) intermediate energy

(c) high energy, above mc^2 for all particles.

For the low energy(a), elastic collisions between the particles and "whole" atoms of the medium are important. In the intermediate energy region, the

principal interaction is between the particle and the atomic electrons of the stopping medium. Electrons are excited into higher quantized energy states(excitation) or continuous energy states(ionization). This inelastic collision process is well understood through Coulomb forces and the stopping power. The average energy loss per unit length of path can be computed from a knowledge of a few parameters measured experimentally. The bulk properties of the material (e.g. density) also influence the interaction process and tend to decrease the stopping power. This phenomenon is called the "density" effect or "polarization" effect. Nuclear interactions occur only rarely(1 per 10^9 electron interactions), but their large effect (i.e, severe energy loss) is of importance for the upper range of intermediate energies(b) of heavy charged particles.

For high energies(c), radiative interactions or "bremsstrahlung" is of major importance.

The interactions of electrons have two distinctive features; (a) For each collision with atomic electrons, large energy losses can occur; and (b) electrons with energies of even only a few hundred keV will be influenced by relativistic effects. In general, it is assumed that after an electron-electron Coulomb collision the emergent electron with the greater energy will be considered the

"primary". The mean energy loss, expressed in units of MeV/cm^2g, is given by the collisional mass stopping power;

$$-\left(\frac{dT}{\rho dx}\right)_{coll} = \left(\frac{0.1535}{\beta^2}\right)\frac{Z}{A}\left[\ln\left\{\frac{2(\tau+2)}{(I/mc^2)^2}\right\} + F(\tau,\Delta) - \delta\right]$$

where $\Delta = \frac{1}{2}\tau$ and

$$F = -1-\beta^2+\ln\left[(\tau-\Delta)\Delta\right]+\left[\tau/(\tau-\Delta)\right] + \frac{\frac{1}{2}\Delta^2+(2\tau+1)\ln\left[1-(\Delta/\tau)\right]}{(\tau+1)^2}$$

Here $\tau = (T/mc^2)$, δ is the density (or polarization) correction, and mc^2 =511,006eV; Δ is the maximum energy transfer of interest in units of mc^2. The above equations were written containing Δ explicitly so that they would be useful in the description of the linear energy transfer(LET) or restricted stopping power(45).

A second important effect for the energy loss of electrons is the emission of photons due to acceleration (or decelleration) of a moving charge. This bremsstrahlung energy loss increases rapidly with an increase in energy of the electrons or atomic number of the absorber. A critical energy, T_c, can be defined at which the energy loss due to

Coulomb collision is equal to loss due to bremsstrahlung;

$$T_c \approx [700/(Z + 1.2)] \text{ MeV.}$$

For human soft tissue, T_c is approximately 85 MeV. An estimate of the ratio, r, of the energy loss due to bremsstrahlung to that due to collisions is given by

$$r \approx (TZ/700).$$

Thus for soft tissue($Z \approx 7$) and electron beams up to 30 Mev, $r \lesssim 30\%$. For "hard" tissue($Z \approx 14$), such as bone, this proportion rises to $\approx 60\%$.

I.2.6 Mass Angular Scattering Power

When a charged particle traverses a slab of finite thickness, it undergoes a large number of collisions, most of which produce very small angular deflections. As a result of these successive collisions and cumulative redirections, one may want to compute the probability that the particle emerges from the slab with a particular lateral displacement and direction.

As a measure of multiple scattering, the ICRU(17) suggests the mean square scattering angle, $\overline{\theta^2}$ and defines the quotient $\overline{\theta^2}/\rho \cdot \ell$ as the "mass angular scattering power" in a manner analogous to mass stopping power. This quantity should be used cautiously, however. The original calculation of Rossi(21) used by ICRU, was based on the validity of superposing numerous small and independent angular deflections. This is generally not the case in multiple successive scattering processes, especially through thick slabs. It is valid only when, for each collision, the direction of the emergent electrons does not differ significantly from the initial direction, and the electrons remain "bunched" and essentially parallel to the incident beam direction. Thus, the appplicability of the mass angular scattering power is confined to such a case as the passage of electrons through an ultrathin plate of scattering medium. This is often overlooked, and many authors continue to misuse this quantity(38,40) for thicker absorbers.

I.3 Electron Beam Treatment Planning

The principle of electron beam treatment planning is simple. The intent is to optimize the treatment of a malignant tumor by delivering the maximum dose to the target volume, while sparing the adjacent healthy tissues.

Thus, the treatment planning process can be regarded as the procedure of getting precise information of the patient anatomy and selecting the optimum field arrangement to administer a prescribed dose distribution.

I.3.1 Description of The Patient

The necessary patient-specific data for treatment planning are the patient's external contour, the internal anatomical structures, and the location of the tumor. From a physical standpoint, these essential data are available through X-ray computerized tomography(CT). It should be also noted that the CT scanner is used to obtain tissue density maps, although the potential exists to also obtain tissue atomic numbers(11).

I.3.2 Dose Distribution

Once the anatomical data for a particular site is acquired, the next step in treatment planning is to select the suitable type of electron beam(s) which will provide the optimum irradiation. The accurate computation of the dose distribution is essential and the method used must be reliable, for a wide range of beam, and patient configurations.

For a tumor located at depth, treatment beams unavoidably deliver undesired radiation to the healthy tissues overlying the tumor in the treatment region. In this context, the skin (surface) dose, relative to the maximum dose has important implications for radiation protection of the healthy tissues. The typical skin or surface dose for a broad beam of electrons is approximately 85% to 95% of the maximum dose, and varies according to the method of producing the macroscopic beam. Electron beams generated by scanning a pencil beam, rather than by foil-scattering, and requring less secondary collimation reduce the skin dose significantly.

I.3.3 Characteristics of Depth Dose Curves

The relative depth dose curve of a broad beam of electrons(see Figure 1) can be divided into several zones of interest; the initial build-up region, the depth of maximum dose, the fall-off of dose, and the "tail" of the curve caused by photon contamination. All of these are influenced by the parameters of the beam, namely, the nominal energy, the field size, the energy spectrum, and the field uniformity and symmetry. What they have in common in influencing the shape of the depth-dose curve is the degradation and redirection of electron energy, that is, the broadening of the energy and angular distribution

of the electron beam.

The initial build-up region of the depth dose curve is where the initial interaction of electrons occur with the scattering medium. This region is subject to the fluence of the incoming electrons from outside of the medium and some electrons backscattered from the deeper regions of the medium. These electrons may also contribute partially to the skin dose, if they manage to reach the surface of the medium. Thus every electron beam, regardless of its size, has a build-up region, even though it is not as evident for a very narrow beam.

The build-up region has a significant meaning in the treatment of the tumors near the skin surface, such as lesions of the ear, lip, and cheek. In these cases, it is advantageous to employ lower-energy beams but it is sometimes still necessary to protect underlying tissues by placing a shield behind the treatment volume. Certain studies have indicated increases, by as much as 80%, due to back-scattered electrons from such lead "shields". This overdosage can be minimized by using a shield constructed of lower atomic number materials, or lining the lead shield with a thin layer of wax(22,23,24). The following explanation can be given for these protective effects. Firstly, the effectiveness of lower atomic number material might be caused by the reduction in the fluence of

backscattered electrons, as confirmed by Baily.(25) The lining effect might be explained by two phenomena happening in the lining and in the lead shield. The electron beam first enters the wax lining, and exits with a high residual energy because the lining is comparatively "transparent". Once this beam enters the lead portion, part of the electrons are backscattered with reduced energy after undergoing multiple scattering in the lead. The lining on the incoming face of the lead shield is then more "opaque" to these lower energy electrons backscattered from the lead and reduce the dose due to backscattering. The above possible explanations are tentative and more understanding of scattering in general is required for validation.

Another significance of the build-up region can be found in the distortion which occurs when the beam is incident obliquely on the surface. In this case, the dose at shallow depths increases and the dose at deeper locations decreases.(26) The increase of relative dose at shallow depth is obvious; while most of the incident electrons are retained in the medium, some of the multiply-scattered electrons can escape through the medium surface; This represents a pure gain for the build-up region and a pure loss for the deeper region.(Figure 4)

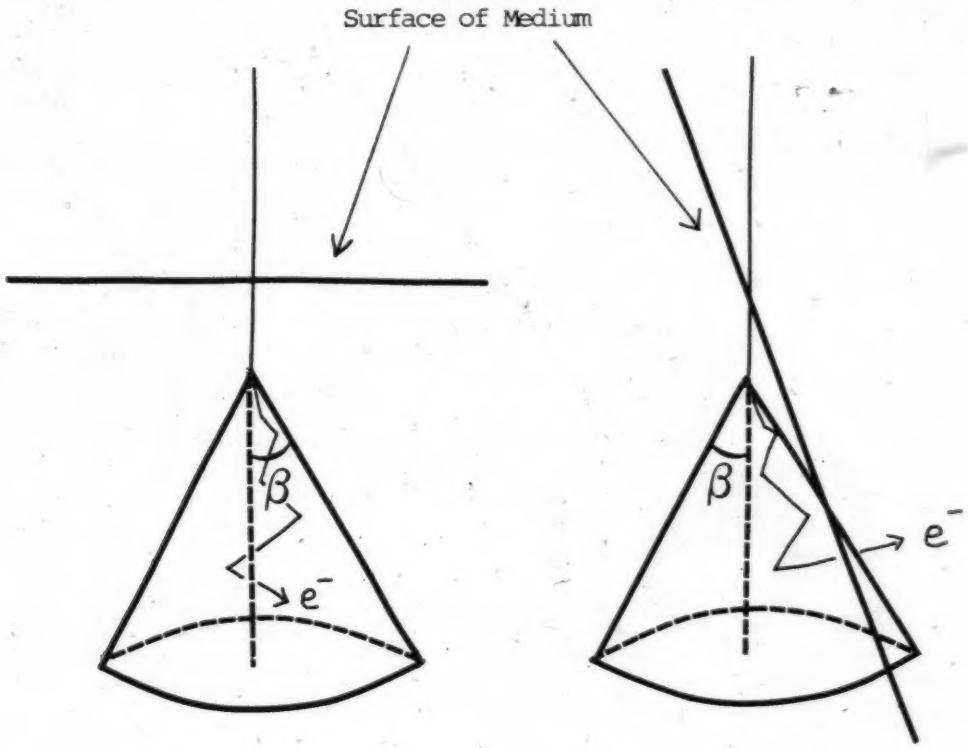

Fig. 4. The effect of tilted surface of a medium on the dose distribution

When the incident beam is sufficently large or the electrons in the beam are sufficiently degraded, the electron beam delivers the maximum relative dose at a certain depth. This depth of maximum dose(dmax) is believed to be the depth where the transport and the loss of electrons are combined to provide a maximum net number of electrons per unit volume.

The dose fall-off region of the depth dose curve is believed to be caused primarily by the stopping of the incident electrons after progressive energy loss. Historically, the implementation of electron beams for radiation therapy was accelerated by the need for a fall-off of dose behind the target volume. For lower energy electron beams, this dropoff is very abrupt and useful for the treatment of superficial or shallow lesions.

For monoenergetic beams produced by a scattering foil and collimation, the production of bremsstrahlung in these devices is unavoidable. The bremsstrahlung usually forms the tail end of the depth dose curve. The relative magnitude ranges up to 10% of the maximum dose, depending on the accelerator energy of electrons. Few experimental studies of this "tail" and its significance on treatment planning have been reported.

I.3.4 Field Shaping

The treatment of tumors with an electron beam sometimes requires considerable shaping of the irradiation area. Lead sheets cut in the shape of the treatment portal are often used in conjunction with the standard circular or rectangular applicators. The thickness of lead shielding is usually chosen to reduce the dose in the "shadowed" region to less than 5% of the dose in the open beam. For high energy electrons additional thickness beyond a few millimeters does not decrease the dose further because of the bremsstrahlung produced.

It is generally suggested that if the field is large and the blocking is minimal, then the normal dose calibration, may be used, but for extensive or complex blocking, a special calibration should be carried out(33).

I.3.5 Isodose Curves

In electron beam treatment planning, isodose distribution data play a key role in that they provide the two-dimensional map of the dose. Information about the dose at off-axis points and at the edges of the collimated beam is thereby obtained. It is common practice to choose a beam(s) so that the target volume lies entirely within

the 80% or 90% isodose curve. However, even in a homogeneous medium, the isodose curves for electron beams produced by foil-scattering are not "flat" so that the area covered by 80% or 90% isodose line is considerably less than that based on the geometric field area defined at the surface.(Figure 5) Therefore, to cover the target area completely, a larger field at the surface is usually used, thereby increasing the irradiation of healthy tissues. This problem can become worse if tissue inhomogeneity is present. For example, the "bulging" of isodose can be accentuated in a low density region.

I.3.6 Interactions in Heterogeneous Tissue

For the energy range(<50MeV) of electrons used in radiation therapy, the most important microscopic interactions of electrons with the constituent atoms of the medium are due to electromagnetic forces. The number of interactions among the incident "bare" electrons is negligible compared with that between incident electrons and atoms of the medium. The two dominant resultant effects of the interactions are deflections and the loss of kinetic energy(21). The deflection takes place when an electron passes in the neighborhood of a nucleus. Since the nucleus is very heavy with respect to the incident electron, the energy of the nucleus does not change

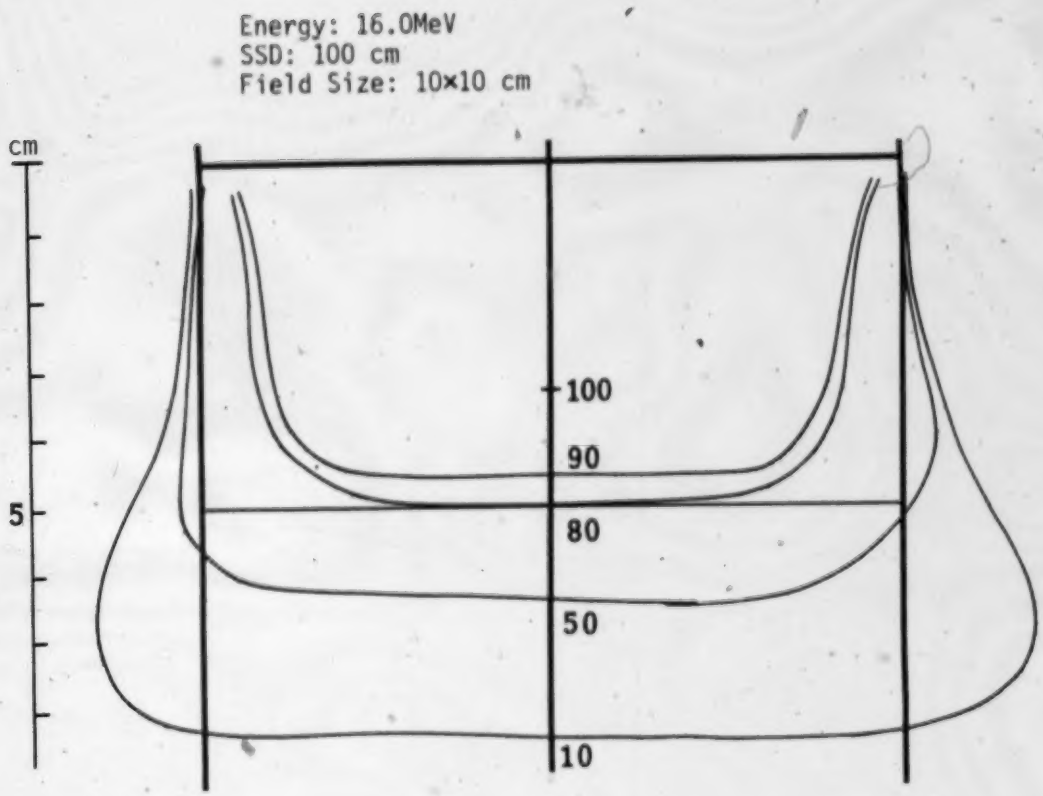

Fig. 5. Constriction of the 80% and 90% isodose line in comparison with the geometric field size (at surface)(33)

appreciably by recoiling and the collision is an elastic one(exclusive of the radiation emitted during the process). The loss of kinetic energy occurs when an incoming electron interacts with one of the atomic electrons having comparable mass.

From a physical standpoint, the inhomogeneities in the irradiated volume can be regarded as a distribution map of materials having high or low density and/or atomic number. In case of human tissues, where there is not a big difference in mass numbers of major constituent atoms(H,C,O,N), the density variations affects multiple scattering of electrons by changing the possible number of scattering events, either elastic or inelastic. That is, the density effects of an inhomogeneity can alter both the gross amount of energy deposition by increasing or decreasing the frequency of inelastic scatterings, and the overall spatial distribution of energy deposition by increasing or decreasing the number of elastic scatterings. These two effects are interrelated since the energy loss of individual electrons by inelastic events affects the elastic scattering which is energy-dependent. The major influences of the atomic number of the material is through dependence in the microscopic scattering cross-section. Since the inelastic scattering cross-section contains the term, Z/A, there is not a big difference in the collisional energy loss in each collision with an orbital electron for

two media of different atomic numbers. On the other hand, the elastic scattering cross-section contains the term, Z^2/A, in which variation of Z can result in a significant effect. The main influence of variation in Z, therefore, is the angular redirection of electrons. In summary, the density effect of the inhomogeneity alters both the gross amount of energy deposited in the finite volume and its spatial distribution, whereas the atomic number mainly alters the latter only.

I.4 Present Theoretical Model for Electron Transport

The interest in the transport of high energy electrons in a scattering medium has been steadily growing ever since the concept of "pencil beam analysis" was proposed by Lillicrap et. al.(41) Some semi-analytic and empirical approaches to the transport problem which had been used previously were not suitable for narrow beams of electrons(47) because they relied on broad beam parameters. These methods are reviewd in chapter II.

A transport equation, currently used widely in medical radiation physics, is that derived by Fermi.(46) This equation was intended for the description of very high energy($\approx$GeV) charged particles passing through a thin slab of scattering medium. Its derivation

involved approximations, which are not necessarily suitable for a thicker media and lower energy beams. The two notable approximations are the assumptions that particles (a) do not lose their energy in crossing a medium, and (b) always travel paraxially along the incident direction. The solutions to the Fermi equation clearly shows the effect of the latter approximation.(46) The resultant angular and spatial distribution functions are Gaussian in shape; the probability that a particle has large angular orientation is negligible. In this work, the problem of electron transport is approached by studying a more general equation, namely the linearized Boltzmann equation.

CHAPTER II

REVIEW OF DOSE CALCULATION METHODS

Accurate calculation of the dose distribution for a specific clinical situation is one of the main steps in electron beam treatment planning. After the introduction of electrons as a mode of radiotherapy, the dose calculation methods have been steadily growing in number as well as in improved accuracy(47). Having started with the assumption of a homogeneous patient, today's dose calculation methods attempt to handle the complex inhomogeneity distribution of tissue in a patient. The advent of X-ray computerized tomography(CT) and the availability of high speed computing facilities stimulated the development of more accurate and yet practical methods of dose calculation.

In general, the early dose calculation methods were developed for application to simple situations. Current trends are towards establishing a flexible method which is

useful for more complex situation in heterogeneous tissue. In the following sections, the major dose calculation methods are reviewed(47).

II.1 Absorption Equivalent Thickness Method

As previously explained in Chapter I, the changes in density and/or atomic number of a scattering medium alter the depth dose curve for a broad beam of electrons. Laughlin (50) discovered some general aspects of these alterations (Figure 6);

(a) Within and beyond tissues of lower density, such as lung, the central axis dose increases, as if the depth dose curve is "shifted" longitudinally towards a deeper location,

(b) Beyond high density regions, such as bone, the dose contours are displaced toward the skin surface with a consequent decreased dose at a given depth.

(c) The magnitude of the actual dose in and beyond low density regions, relative to that in a unit density medium, depends in a nonlinear manner on the location, extent, and density of the inhomogeneous region.

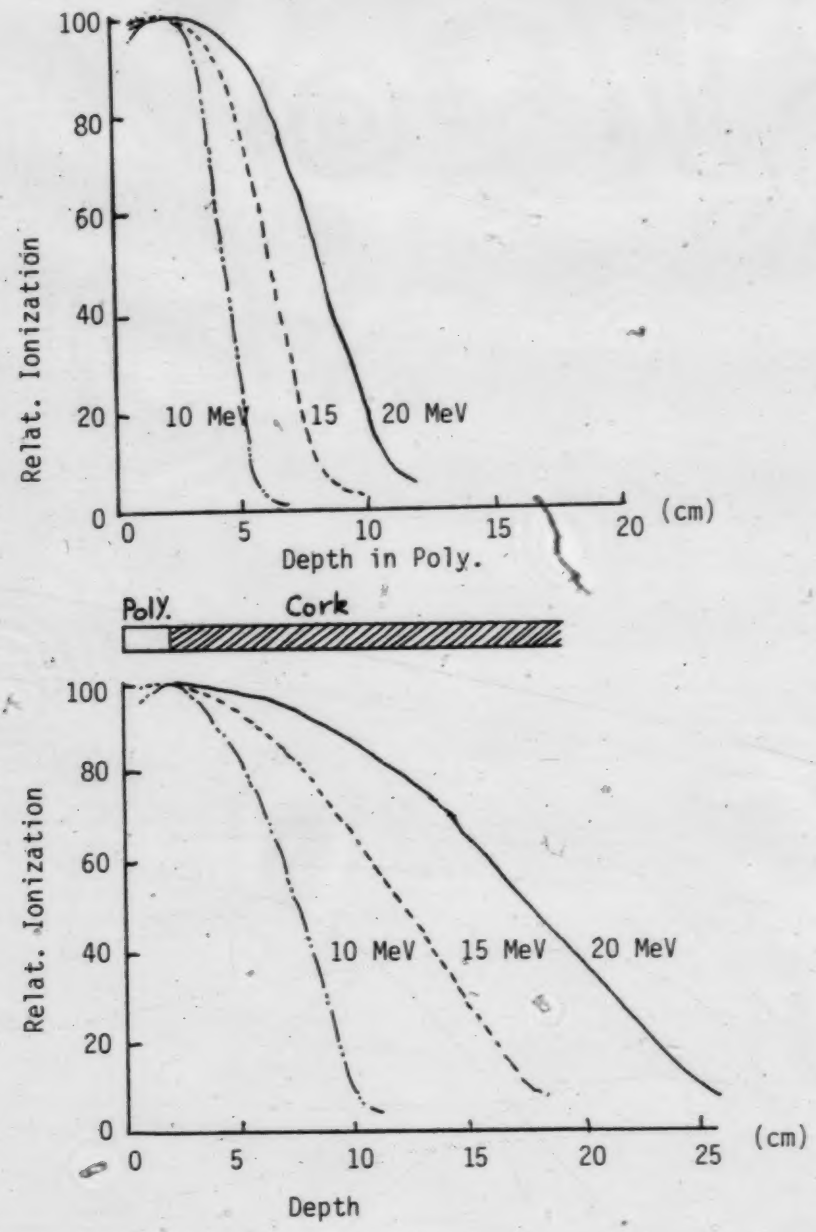

Fig. 6. Central-axis depth dose distribution produced in (above) high-impact polystyrene and (below) 2.0 cm high-impact polystyrene followed by cork, by electron beams of indicated energies. (6)

(d) Within high atomic number materials, such as bone, and immediately beyond the interface region there can be regions of elevated dose ("hot spots").

A correction factor has been developed to take into consideration the presence of inhomogeneities and is referred to as the absorption equivalence thickness (AET) method. Although the correction factor should depend on depth, for practicality, an average factor is used based on the following relations;

$$AET = 1.3\,\rho_l$$

where ρ_l is the assumed lung density. For bone,

$$AET_{bone} = \frac{\rho_b}{1.0\ g/cm^3}\ \frac{\text{(electrons/g in bone)}}{\text{(electrons/g in water)}}$$

$$= \frac{\rho_b}{1.0\ g/cm^3}\ \frac{3.0\times10^{23}/g}{3.36\times10^{23}/g}$$

$$= 0.88\,\rho_b$$

where ρ_b is the density of a bone.

The correction of an isodose distribution in a homogeneous medium using the AET factor is usually made by assigning AET factors to each inhomogeneous region along divergent rays from the virtual source. The corrected isodose distribution can be obtained by joining equal dose

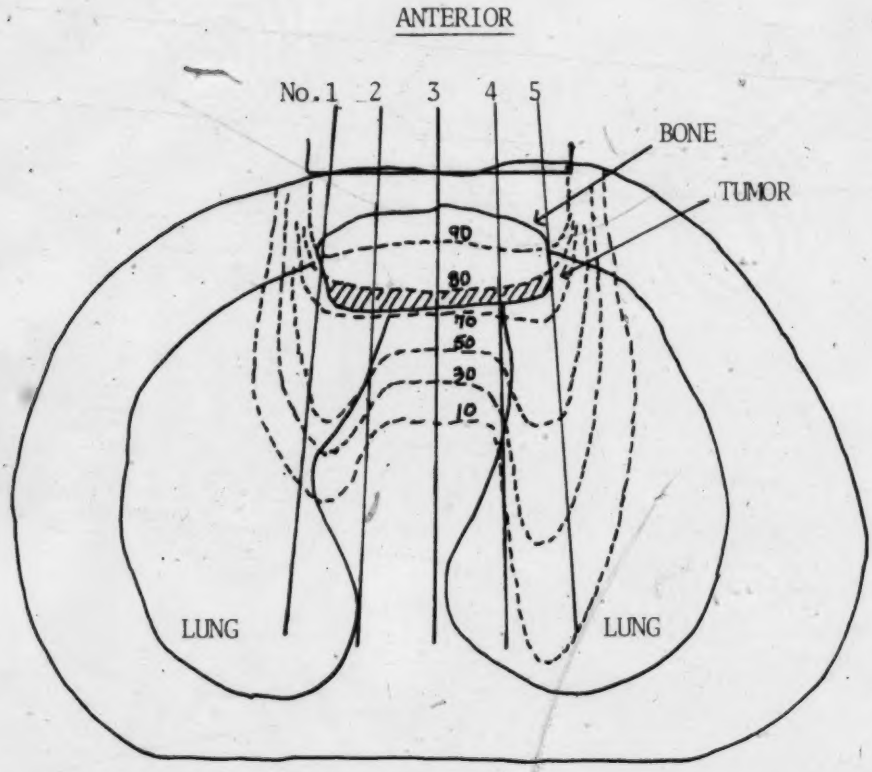

Fig. 7. Calculation of isodose distribution with correction for bone and lung inhomogeneity. (50)

II.2 Coefficient of Equivalent Thickness (CET) Method

Another way to determine the dose distribution in lung uses an appropriate correction factor, called Coefficient of Equivalent Thickness(CET), which can be defined by referring to Figure 8. Considering, first, the case where there is no divergence of the beam, the coefficient of equivalent thickness is defined as the ratio of the distance in the water to the distance in the inhomogeneity, as measured from the interface, at which we have the same percent depth dose value.

$$CET = x_1 / x_2$$

where

$$y_{d_2}(x_2) = y_{d_1}(x_1)$$

Here, y refers to percent depth dose, X to the distance measured from the interface, and 1 and 2 refer to the standard water curve and water-cork curve, respectively. These have to be measured experimentally.

Now the decreasing part of the curve in water can be described by the empirical equation(51);

$$y = 110 - 10e^{\mu x}$$

where x is measured from the depth of the 100% point on the central-axis depth dose curve. The value can be calculated from the standard water curve;

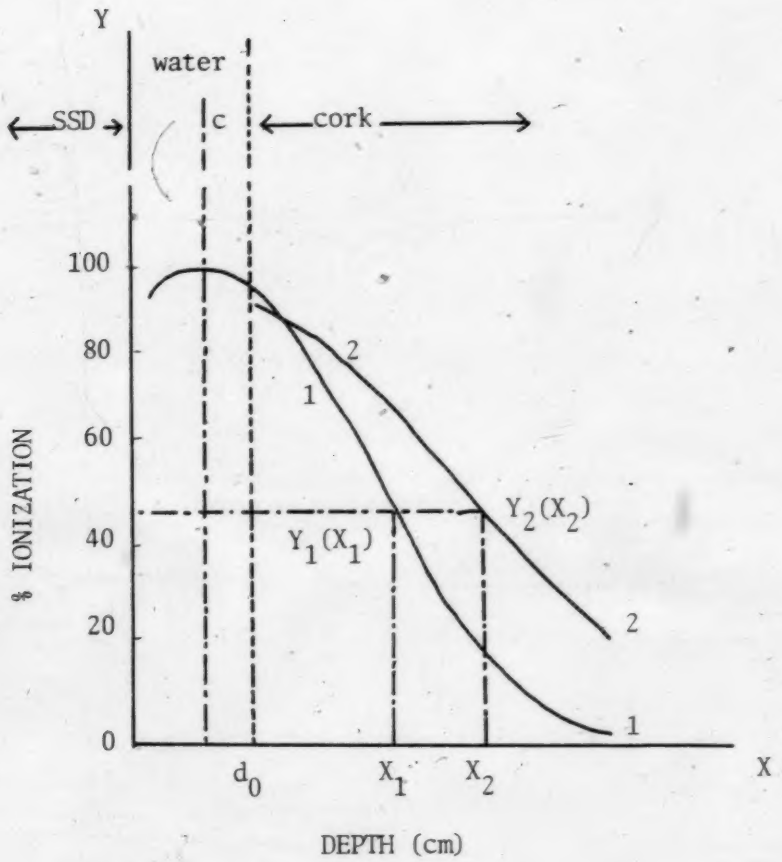

Fig. 8. Coordinates and parameters used for the calculation of CET and MAC methods. (47)

$$y_1(x_1) = 110 - 10\,e^{\mu(x_1 + c)}$$

where c is the distance between the interface and the depth of the 100% point(dmax) on the water curve; c can be either positive or negative;

$$y_2(x_2) = 110 - 10\,e^{\mu(x_2 \cdot CET + c)}$$

For a given ray, there will be an inverse square correction given by

$$S = \left(\frac{SSD + d_o + CET \cdot x_2}{SSD + d_o + x_2} \right)$$

and $y_2(x_2) = y_1(x_1) \cdot S$ Thus, the overall expression is;

$$y_2(x_2) = \left\{ 110 - 10\,e^{\mu(x_2 \cdot CET + c)} \right\} \left\{ \frac{SSD + d_o + CET \cdot x_2}{SSD + d_o + x_2} \right\}^2.$$

Since y_2 is measured at x_2, μ can be found from the water depth dose curve, and since SSD, d_o, and c are known, the equation can be solved for CET.

As in the AET method described previously, the beam can be divided into seperate rays, a new attenuation coefficient μ and values for x and d_o measured, and the corrected doses calculated along each ray.

II.3 Modified Absorption Coefficient (MAC) Method

To implement the CET method with consideration for the polarization effect, field size dependence, deviation of central axis percent depth data from Laughlin's equation(51) at electron energies above 20 MeV, and the variation in the densities of internal organs for the specific patient, Bagne(52) introduced the Modified Absorption Coefficient(MAC) Method.

For a given percentage depth dose measured in a water-cork phantom at a distance X_2 from the interface, the MAC value is defined as (see Figure 8);

$$MAC = X_1 \rho_1 / X_2 \rho_2$$

where

$$y_2(x_2) = y_1(x_1) \cdot S$$

and

$$S = \left(\frac{SSD + d_o + MAC \cdot X_2 \rho_2 / \rho_1}{SSD + d_o + X_2} \right)^2 .$$

Here, the water and cork densities are designated by ρ_1 and ρ_2, repectively, and S is the inverse square correction factor.

Although percentage depth dose curves for energies $\leq$ 20 MeV follow Laughlin's equation, data obtained for higher energies deviate significantly from a straight line at values below the 50% percent depth dose level(52). Bagne suggested a modified equation based on curve fitting;

$$I(x) = 110 - 10\exp\{\mu[(x-d_m)\rho - \lambda(x-d_m)^3\rho^3]\},$$

where ρ is the density of the medium and λ is the depth dose correction coefficient. Regardless of field size, λ is constant for a given material and energy. For energy $\leq$ 20 MeV, λ approaches zero.

The percentage depth dose at a given point in water is then obtained as;

$$y_{d_1}(x_1) = \left(110 - 10\exp\{0.693 n\rho_1[1-\lambda(x_1-c)^2\rho_1^2]\}\right)P,$$

where P is the correction for the polarization effect, c is the distance between the 100% depth dose point and the surface-interface distance, and n is defined as;

$$n = (x-d_m)/(d_{90}-d_m)$$

Then, $y_{d_2}(x_2)$ can be expressed in the following way using the MAC method;

$$y_{d_2}(x_2) = \{110 - 10\exp[0.693\, ED/(d_{90}-d_m)]\}SP,$$

where

$$ED = (MAC\cdot P_2\cdot x_2 - CP_1) - \lambda(MAC\cdot P_2\cdot x_2 - CP_1)^3$$

II.4 Correction Method for Edge Effects

For the determination of the dose perturbation at the edge of a finite inhomogeneity, Pohlit(54) introduced a correction method based on experimental observations. In order to quantify the limit of influence of the edge, Pohlit graphically defined two angles α and β, which are dependent on the mean electron energy $\bar{E}$ (Figure 9 and Figure 11);

$$\bar{E} = E_o (1 - z/R_p),$$

where

E_o = initial energy,

R_p = practical range,

z = depth in medium.

The maximum change, P_{max}, of absorbed dose due to an edge between different kinds of medium is (Figure 10);

$$P_{max} = \frac{D_{max} - D_o}{D_o}$$

where D_{max} is the absorbed dose at the highest increase or depression due to the presence of the edge and D_o is the absorbed dose at the same point in the absence of the edge.(Figure 11) Whenever edges are present in the irradiated volume, the dose can be corrected along the angles α and β.

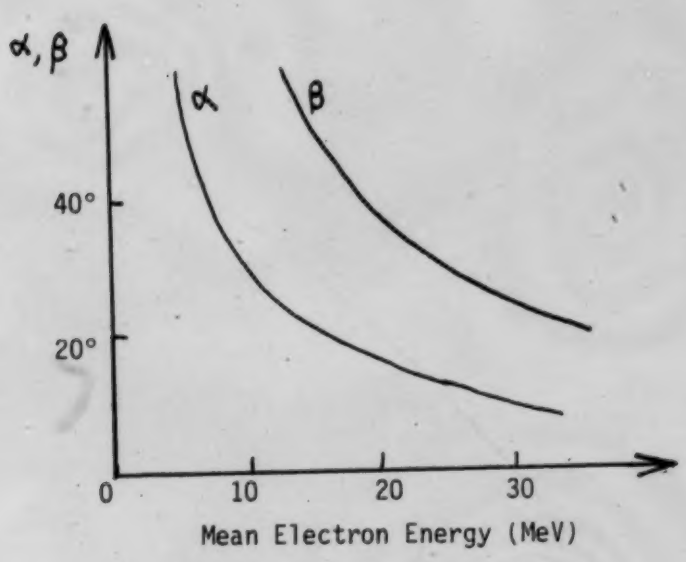

Fig. 9. Energy dependence of the angles α and β. (54)

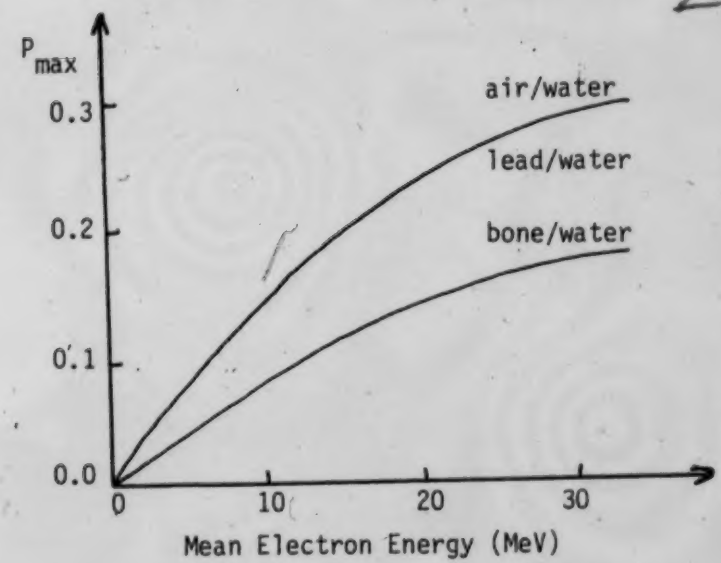

Fig. 10. Maximum changes in absorbed dose behind edges. (54)

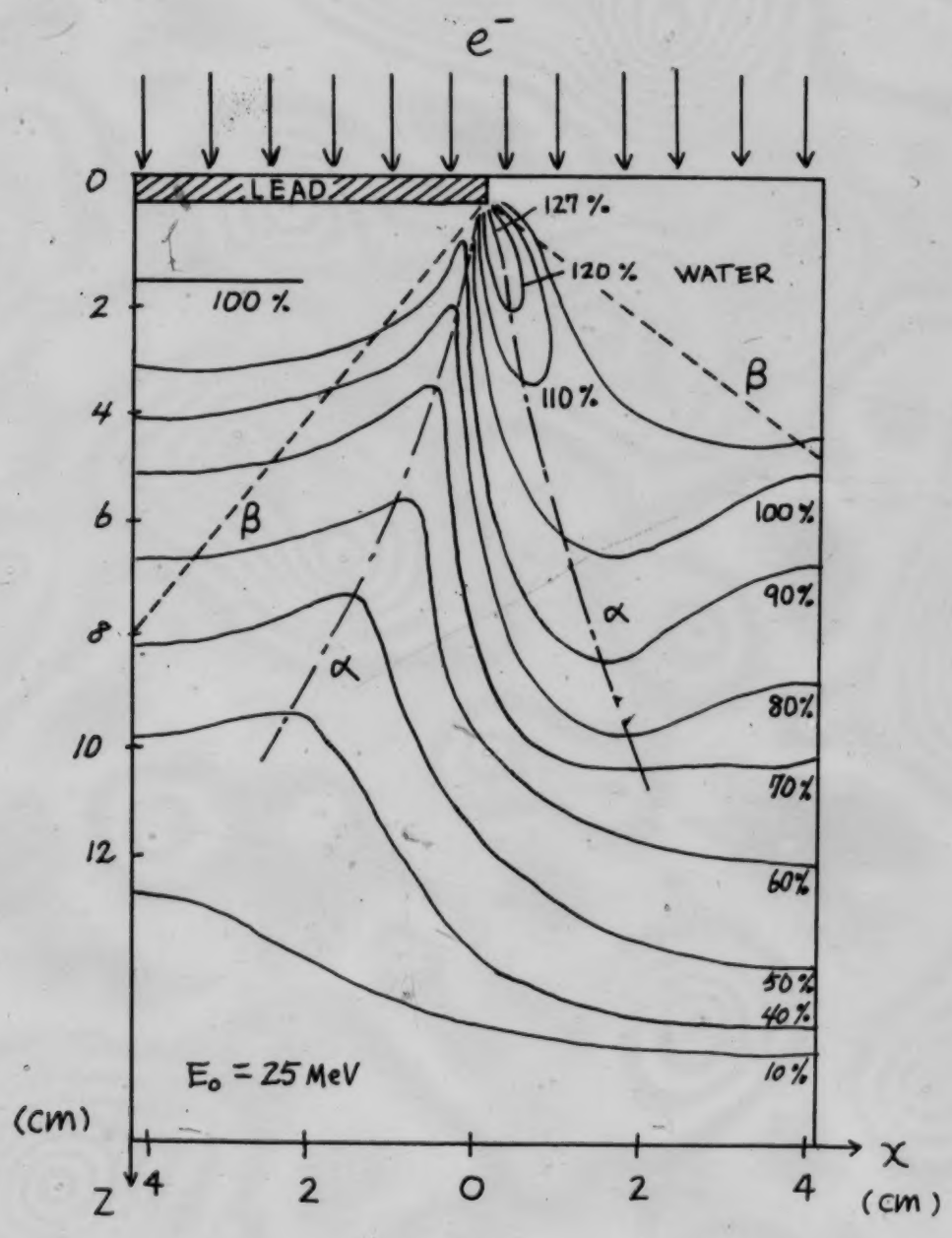

Fig. 11. Measured dose distribution behind a lead strip in a water. (54)

II.5 Approximation of Isodose Curves by the Age Diffusion Solution

For the accurate characterization of the dose distribution of rectangular electron beams with minimal amount of empirical data, the solution to the age-diffusion equation can be used to approximate the dose distribution, at least in a homogeneous medium(36).

One typical example is(see Figure 12);

$$D(x,y,z,\tau) = \frac{D_o}{z}\left[\operatorname{erf}\left\{\frac{x_o(z)-x}{2(k\tau)^{1/2}}\right\} + \operatorname{erf}\left\{\frac{x_o+x}{2(k\tau)^{1/2}}\right\}\right]$$
$$\times\left[\operatorname{erf}\left\{\frac{y_o(z)-y}{2(k\tau)^{1/2}}\right\} + \operatorname{erf}\left\{\frac{y_o+y}{2(k\tau)^{1/2}}\right\}\right]$$
$$\times \cos\left[G_1(z/R_p)^2 + G_2(z/R_p) + G_3\right]$$
$$\times\left[F/(F+z)\right]^2 \times \exp\left[-(2\pi/3R_p)\cdot(k\tau)^{1/2}\right]^2,$$

where

$D(x,y,z,\tau)$ = dose at depth z,

$(k\tau)^{1/2} = (Cz/R_p + P)^N$,

F = source-skin distance,

$x_o = (1/2)(\text{width} + K_e)\cdot[(F+z)/F]$,

$y_o = (1/2)(\text{length} + K_e)\cdot[(F+z)/F]$,

R_p = practical range,

G_1, G_2, G_3, C, N, P = constant for a given energy.

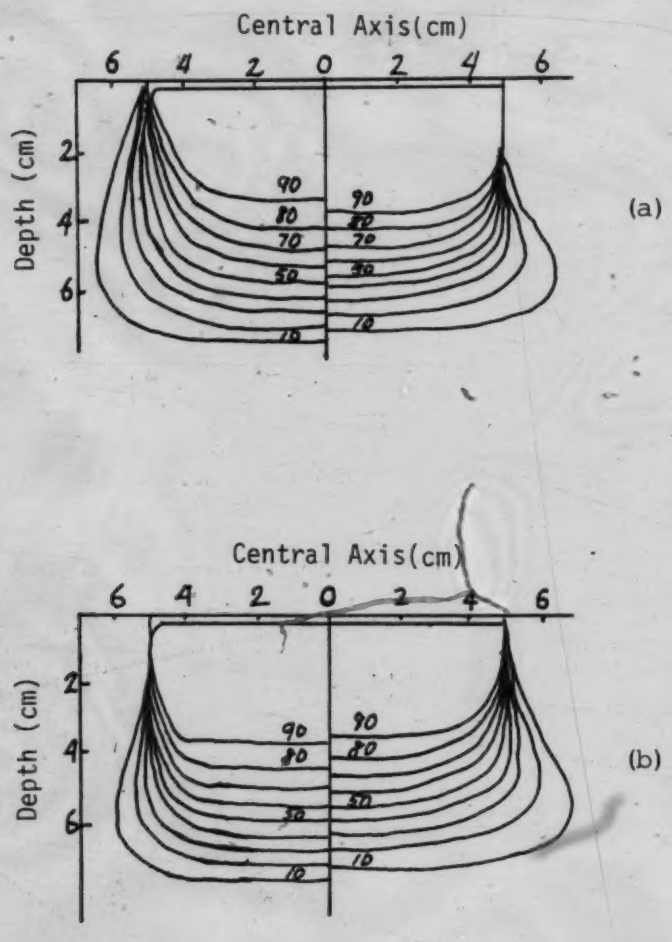

Fig. 12. Calculated isodose distributions in water, assuming a monoenergetic incident electron energy of 15 MeV and a field size of 10 cm with a parallel beam. The values of c and n are: (a) Left side, c=1.5,n=1.0 Right side, c=1.5,n=3.0 (b) Left side, c=1.2,n=2.0. Right side, c=1.8,n=2.0. (36)

All the contants are to be "adjusted" to give a good fit to the experimental data. The functions of individual parametric constants are; P characterizes the beam diffuseness at the surface; C characterizes the increase in diffuseness with depth; N is an overall shape-changing parameter; K_e adjusts the width and length of rectangular beams. This method is used on some commercial treatment planning computers(e.g., AECL TP-11), but no allowence are made for tissue inhomogeneity.

II.6 Pencil Beam Analysis of Broad Beam

Unlike most of the dose calculation methods, discussed previously, pencil beam analysis method deals with a broad beam of electrons not as a whole but as an integration of a number of narrow beams (Figure 13). In this way, dose calculation problem becomes a study of a narrow beam of electron which is simpler in many aspects (e.g., mathematical treatment) and can be used to account for small inhomogeneities.

As an analytic expression for a narrow beam, authors have used a solution to the Fermi equation(55,56).

$$f(\theta_x, X, z) = \frac{\exp\left\{-\dfrac{\overline{\theta^2}(z)X^2 - 2\,\overline{r\theta}(z)X\theta_x + \overline{r^2}(z)\theta_x^2}{\overline{\theta^2}(z)\,\overline{r^2}(z) - \left[\overline{r\theta}(z)\right]^2}\right\}}{\pi\left\{\overline{\theta^2}(z)\,\overline{r^2}(z) - \left[\overline{r\theta}(z)\right]^2\right\}^{1/2}}$$

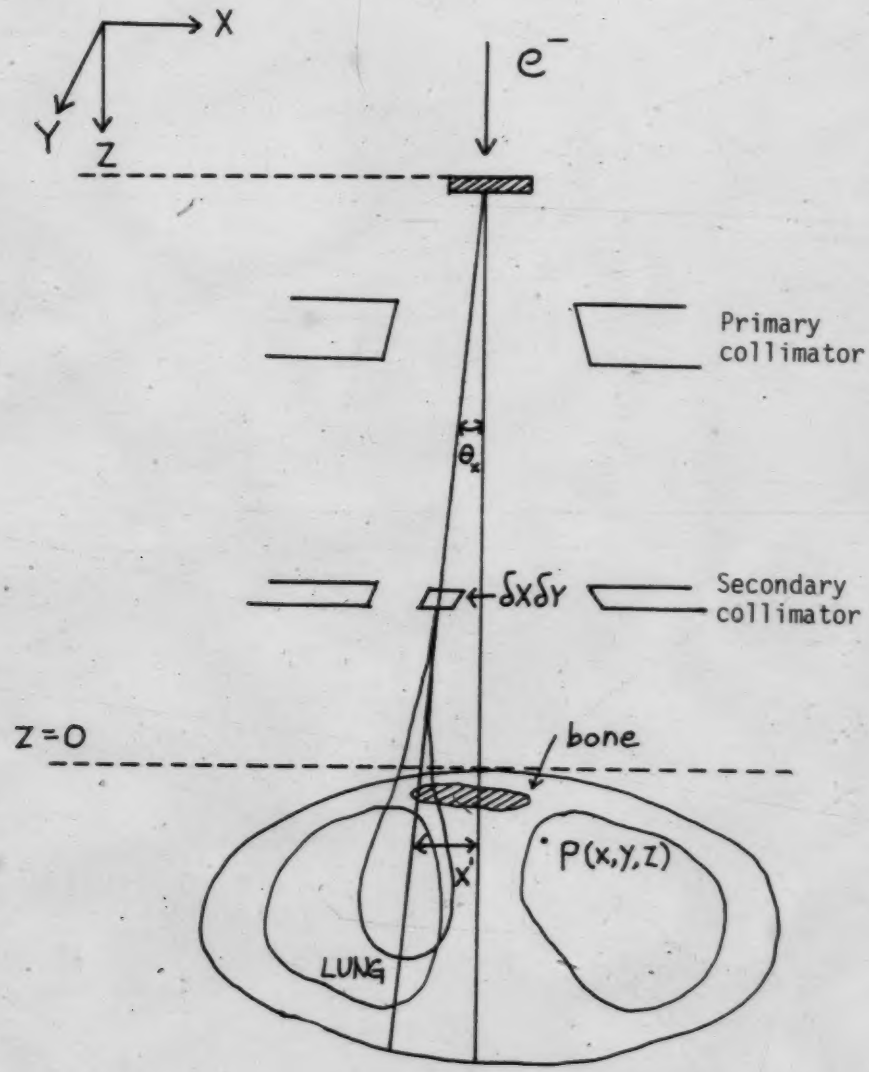

Fig. 13. Schematic representation in the X-Z plane of a therapeutic electron beam incident on a patient. (38)

where

$$\overline{r^2}(z) = \overline{r^2}(0) + 2\,\overline{r\theta}(z)\,z + \overline{\theta^2}(0)\,z^2 + \int_0^z (z-u)^2\,T(u)\,du$$

and

$$\overline{r\theta}(z) = \overline{r\theta}(0) + \overline{\theta^2}(0)\,z + \int_0^z (z-u)\,T(u)\,du$$

With this solution as a basis, a broad beam of electrons can be represented mathematically as a convolution;

$$\Phi(x,y,z) = \iint_S A(x',y',z')\,f(x'-x, y'-y, z'-z)\,dx'dy'$$

where $A(x',y',z')$ is the incident beam fluence and S is the cross-sectional area of the broad beam.

II.7 Summary

As mentioned earlier, the earlier dose calculation methods, such as, AET, CET, MAC mehtods, were developed for a specific treatment situation in which laterally broad inhomogeneities are present in the treatment volume(e.g., lung). Accordingly, the applicability of those methods to a more complex situation(e.g., small voxels of inhomogeneity) remains questionable, even though some

institutions accept these methods to develop a "comprehensive" electron beam treatment planning system(52,55). Furthermore, the empirical nature of the approaches to the problem of these methods makes their application to a "beam model" for computerized treatment planning difficult. This trend is also true for Pohlit's correction method for the edge of an inhomogeneity and Kawachi's isodose calculation method.

Considering these limitations, the pencil beam analysis of broad beam has two distinctive advantages for the computerization of electron beam treatment planning. First, it would require only a minimum amount of empirical data for characterization of the electron beam from a particular medical accelerator. Secondly, as the broad beam is considered to be made up of a number of narrew beams, the treatment of inhomogeneities can be done on a voxel by voxel basis, using CT data. However, at current stage, the necessary theoretical model for the transport of a narrow beam, even in a homogeneous medium, is not well established. The only present model we have is Fermi's model which is quoted in section II.7. This model, for example, ignores the existence of backscattered electrons(see Chapter II). Furthermore, before we can use the pencil beam analysis as a "dose" calculation method, the relationship between the electron fluence distribution and the resultant dose distribution should be well

established, because theory only provides the electron fluence distribution.

CHAPTER III

TRANSPORT OF ELECTRONS IN A SCATTERING MEDIUM

III.1 Introduction

The physical problems in electron radiation therapy are largely due to the beam production techniques commonly used. For instance, the scattering foil, beam-defining collimator, and added shielding materials are used to shape a field but these materials degrade the beam. This is at the origin of two of the most important current problems, that is, tissue inhomogeneity and dose standardization.

From a physics standpoint, the tissue inhomogeneities are local clusters of material which have a mass density and/or atomic number different from that of water. These clusters are usually small in size compared to the electron beam dimension, and yet are not negligible in size. The absorbed dose depends on the relative location of the inhomogeneities, with respect to a point of

interest. The assessment of the influence of the inhomogeneities on a broad-beam of electrons is very difficult. Even after assuming that the required perturbation effect of the inhomogeneity is characterized empirically, current schemes of electron dose computation do not have the necessary foundation to predict these effects and provide guidance for dose compensation. Currently compensation for inhomogeneities is only achieved approximately by selecting an appropriate electron beam energy at the cost of other advantage(e.g., skin-sparing).

The problem of standardization is as serious as the problem of inhomogeneity. Without standardization there is restricted sharing of physical or clinical results because measurements taken on one medical accelerator with the "same energy" may not be relevant to another. Beam spreading by a scattering foil was developed without serious consideration of electron transport and makes it very difficult to develope shareable data bases of "standard electron beams".

Recently, several attempts were made to understand the characteristics of the dose distribution of a broad beam of electrons by decomposing it into a number of narrow beams.(40,41) This type of analysis is advantageous as a method of understanding the inhomogeneity effect. The lateral size of a pencil beam is virtually zero at the

surface of a medium, and does not increase significantly at depth in comparison with the size of inhomogeneities. Therefore, assuming the synthesis of a broad beam from a finite number of pencil beams is valid, we need not be concerned with the lateral dimension of the inhomogeneity; every inhomogeneity can be seen to be "slab-like", relative to an incident pencil beam size.

Pencil beam analysis can also be applied to minimize the problem of standardization. The common origin of this problem is the mechanism of producing a broad beam of electrons which degrades the electrons to such an extent that the characterization of the broad beam becomes ambiguous. However, the characterization of monodirectional and monoenergetic pencil beams which compose the degraded broad beam should be possible in a unique way, because the degree of degradation of electrons within each pencil beam would be independent and not too severe.

III.2 Some Aspects of Electron Transport in a Scattering Medium

All the electrons in a therapeutic electron beam lose their initial energy in a stopping medium, namely, the tissue of a patient. While losing energy through numerous

inelastic collisions, the electrons are also deflected by elastic collisions with the nucleus. These two events are interdependent because of progressive degradation in electron energy and angular distribution of the electron fluence in a scattering medium. In the following section we will discuss some features of these combined effects.

III.3 Multiple Scattering and the Linearized Boltzmann Equation

Basically, the electron transport problem in medical radiation physics is that of an infinite absorber. It is assumed that electrons, in general, participate in a large number of collisions before they are finally stopped. In this calculation we assume;

(a) statistical fluctuations("straggling") in electron range and energy-loss are ignored.

(b) all the collisions between electrons and atoms are assumed to occur instantaneously and elastically. However, the mean energy loss over a finite path-length will be considered.(see section II.3.3.)

(c) bremsstrahlung production by elastic collisions is ignored.

If we rely on the conservation of electrons within an

infinitisimal volume element of phase space, then the linearized form of the Boltzmann equation is;

$$\frac{\partial f}{\partial \ell} + \hat{v}\cdot\vec{\nabla} f = n\int d\hat{v}'\,\sigma(\hat{v}\cdot\hat{v}',\ell)\left\{f(\vec{x},\hat{v}',\ell)-f(\vec{x},\hat{v},\ell)\right\} \quad (II.1)$$

where $f(\vec{x},\hat{v},\ell)d\vec{x}\,d\hat{v}$ is the expected number of electrons in the volume element $d\vec{x}$ about the point $\vec{x}$, whose velocities lie in the range of $d\hat{v}$ about $\hat{v}$, at pathlength ℓ. n is the number of scattering centers per unit volume of medium. $\sigma(\hat{v}\cdot\hat{v}',\ell)$ is the differential scattering cross-section. Here the scattering centers are assumed fixed in position, spherical, and uniformly distributed in the medium. Thus, elastic scattering cross-section only depends on the angle between the trajectories of incident and emergent electrons, $\cos^{-1}(\hat{v}\cdot\hat{v}')$. The general solution to equation(II.1) is uniquely determined if proper boundary conditions are specified. The existence theorem of a solution in a very general case and many more useful properties of equation (II.1), have been studied by Case and Zweifel.(42) Since the equation (II.1) is linear, it is clear that the solution for a broad surface boundary condition can be established by the superposition of solutions with "point" boundary conditions on that surface. In our study, we are interested in the solution to equation(II.1) with the pencil or point boundary condition

on the surface of semi-infinite homogeneous medium. In our discussion, we will assume that the pencil beam is monoenergetic, monodirectional, and incident perpendicularly on the medium surface. In this geometry, the cylindrical coordinate system (ρ , z) without an azimuthal angle for spatial coordinates is suitable. For velocity direction coordinates, $\hat{v}$, spherical coordinates will be used throughout discussion. The azimuthal angle of velocity coordinates is defined as the angle between the ρ-z plane and the projection of $\hat{v}$ on the Z-plane. The incident direction is chosen along the Z-axis.

III.3.1 Fokker-Plank Approximation At Shallow Depth

Supposing that the scattering angle $\cos^{-1}(\hat{v}\cdot\hat{v}')$ is very small, the collision integral within equation(II.1) can be approximated by expanding $f(\vec{x},\hat{v},\ell)$ in a Taylor series about $\hat{v}'=\hat{v}$, retaining only the lowest nonvanishing terms. If we substitute $\cos\theta \equiv \mu$, we find

$$\frac{\partial f}{\partial \ell} + \hat{v}\cdot\vec{\nabla} f = \frac{1}{D}\left\{ \frac{\partial}{\partial \mu}(1-\mu^2)\frac{\partial f}{\partial \mu} + \frac{1}{1-\mu^2}\frac{\partial^2 f}{\partial \varphi^2}\right\} \qquad (II.2)$$

where the "diffusion length", D, is defined by

$$\frac{1}{D} = \frac{2\pi n}{4}\int_0^{\pi} \psi^2 \sigma(\psi)\sin\psi\, d\psi$$

where $\psi = \cos^{-1}(\hat{v}\cdot\hat{v}')$

In order to estimate the error involved in this approximation, we consider an electron perpendicularly incident on the surface of a medium. For simplicity we concentrate on the probability that the velocity of this electron has a polar angle θ at pathlength ℓ without regard to the spatial coordinates. Throughout the rest of discussion we shall be concerned only with path length ℓ small compared to the diffusion length D of the medium. For $\ell \ll D$, it is expected that $f(\theta, \ell)$ will be peaked at small angle θ ; and in the small scattering angle approximation, the equation (II.2) is solved by

$$f_{F\text{-}P} = \frac{1}{\pi \bar{\theta}^2} \exp\left(-\theta^2/\bar{\theta}^2\right) \qquad \text{(II.3)}$$

where

$$\bar{\theta}^2 = 4\ell/D \ll 1 . \qquad \text{(II.4)}$$

It is assumed that the energy of the particle does not change too much during the collisions if $\ell \ll D$ .For a simple assessment of error, we compare solution (II.3) to the true solution of the Boltzmann equation, using an iterative test. By inserting (II.3) into the collision integral of the Boltzmann equation, we find, with the small angle approximation,

$$\frac{\partial f}{\partial \ell}(\theta,\ell) = \frac{n}{\pi\bar{\theta}^2}\exp\left(-\theta^2/\bar{\theta}^2\right)\int_0^{2\pi} d\varphi \int_0^{\pi} d\psi \sin\psi\,\sigma(\psi)$$

$$\times\left\{\exp\left[-(\psi^2 - 2\theta\psi\cos\varphi)/\bar{\theta}^2\right] - 1\right\} \qquad (\text{II}.5)$$

In the Fokker-Plank approximation to the collision integral, the above equation reduces to;

$$\frac{\partial f_{F\text{-}P}}{\partial \ell}(\theta,\ell) = \frac{n}{\pi\bar{\theta}^2}\exp\left(-\theta^2/\bar{\theta}^2\right)\cdot\frac{2\pi}{\bar{\theta}^2}\left(1-\frac{\theta^2}{\bar{\theta}^2}\right)\int_0^{\pi} d\psi\,\psi^2\sin\psi\,\sigma(\psi) \qquad (\text{II}.6)$$

We can say that the Fokker-Plank approximation is appropriate, for a given θ and ℓ, if (II.6) adequately approximates (II.5).

The equation (II.2) can obviously be meaningful only if the scattering cross-section falls off sufficiently abruptly with increasing ψ. In the present discussion, we restrict our considerations to scattering cross-sections which fall off monotonically with increasing ψ and which have the property that there exists some critical angle such that

$$\int_{\psi_0}^{\pi} d\psi\,\psi^2\sin\psi\,\sigma(\psi) \ll \int_0^{\psi_0} d\psi\,\psi^2\sin\psi\,\sigma(\psi) \qquad (\text{II}.7)$$

Under this condition, it is clear that one necessary condition for validity of the Fokker-Plank approximation is

$$\overline{\theta^2} = 4\ell/D \gg \psi_0^2 \qquad (II.8)$$

That is, the approximation is dependable only after a sufficient time has elapsed. Physically this means each electron must have suffered enough collisions before they can be effectively described by the equation (II.2). After the first mean collision time interval, the true distribution should already be "filled out" to a value of order ψ_0. Thus, enough time is needed for $(\overline{\theta^2})^{1/2}$ to exceed ψ_0, that is, for the orientations to be relatively random or "diffuse". It should be also noticed that the expansion of equation (II.5) to terms linear in ψ^2 is incorrect unless

$$\theta \ll \overline{\theta^2}/\psi_0 \qquad (II.9)$$

which is a necessary condition for the Fokker-Plank approximation to be adequate. This condition too has a physical significance. A typical collision involves a scattering through angle of order ψ_0. In a sequence of N collisions, with random changes in azimuthal angle, the mean net deflection angle $(\overline{\theta^2})^{1/2}$ is given by $N^{1/2}\psi_0$. On the other hand, the improbable sequence of such collisions in which the velocity vector remains essentially in a fixed plane yields a net angular deflection $\theta \approx N\psi_0$. Such a coherent chain of scatterings is <u>not</u> properly accounted for in Fokker-Plank approximation. We therefore expect the solution to

equation (II.2) to become invalid when $\theta > N\psi_0 \approx \bar{\theta}^2/\psi_0$. While conditions (II.8,9) are necessary for securing the validity of the Fokker-Plank approximation, the sufficiency is provided by a simple obvious condition;

$$\theta^2 < \bar{\theta}^2 \qquad \text{(II.10)}$$

as one expects on physical grounds and can verify by inspection of equation (II.6). For an improved estimate of this sufficient condition, we inquire about the contribution to $f(\theta, \ell)$ for $\theta^2 \gg \bar{\theta}^2$. This contribution comes from a single large angle scattering having taken place during the path length interval ℓ . Since the major contribution to the probability distribution comes from the deflection angles up to a value of order $\bar{\theta} \ll \theta$, such a scattering must involve an angular deflection which is essentially equal to θ itself. Hence, this single scattering contribution is approximately given by

$$f_s(\theta, \ell) \approx 2\pi n \ell \sigma(\theta) , \qquad \theta \gg \bar{\theta} \qquad \text{(II.11)}$$

Note, from (II.4) and (II.11), that

$$f_s / \bar{\theta}^2 = (2\pi n/4) D\sigma(\theta) \qquad \text{(II.12)}$$

and from the definition of D , that

$$1/D \gtrsim (2\pi n/4)\,\psi_o^4\,\sigma(\psi_o) \qquad (II.13)$$

Now, from the single large angle scattering probability, we can calculate the total probability $P_T(\theta,\ell)$ for single scattering through angles of order θ or larger by simple integration over angle θ. Since $\psi_o \ll \bar{\theta} \ll \theta \ll \pi$, and supposing that $\theta^4\sigma(\theta)$ is a monotonically decreasing function, we have

$$P_T(\theta,\ell) = \frac{\pi n}{2}\,\bar{\theta}^2 D \int_\theta^\pi \sigma(\theta')\sin\theta' d\theta'$$

$$\approx n\bar{\theta}^2 D\theta^2\sigma(\theta) \lesssim \frac{\bar{\theta}^2}{\theta^2}\,\frac{\theta^4\sigma(\theta)}{\psi_o^4\sigma(\psi_o)} \ll 1 \qquad (II.14)$$

Therefore, we can safely neglect multiple large angle scattering for all $\theta \gg \bar{\theta}$. However, single large angle scattering can be neglected only when $f_s(\theta,\ell) \ll f_{F\text{-}P}(\theta,\ell)$. The equation (II.2) is then adequate provided θ satisfies (II.9) and is also less than a critical angle, θ_c, determined by $f_{F\text{-}P}(\theta,\ell) \ll f_s(\theta,\ell)$. Thus,

$$\frac{1}{\pi\bar{\theta}^2}\exp\left(-\theta_c^2/\bar{\theta}^2\right) \approx 2\pi n \ell\,\sigma(\theta_c) \qquad (II.15)$$

or from (II.4) and (II.13);

$$\exp\left(-\theta_c^2/\bar{\theta}^2\right) \approx \pi\left(\bar{\theta}^2/\psi_o^2\right)^2\left(\psi_o^2/\theta_c^2\right) \qquad (II.16)$$

These results can also be understood from a direct comparison of equations (II.5) and (II.6). For $\theta \gg \bar{\theta}$, the expression in curly brackets in (II.5), regarded as a function of ψ, has a sharp peak of height $\approx \exp(\theta^2/\bar{\theta}^2)$ and of width $\approx \bar{\theta}$, centered at $\psi = \theta$. In the integral on the right hand side of equation (II.6) this makes a contribution which is of the order of $f_s(\theta,\ell)/\ell$; i.e., it is just the contribution of a single large angle scattering. Indeed, if the condition (II.9) is satisfied, the right side of equation (II.5) is essentially the sum of two terms;

$$\frac{\partial f}{\partial \ell} \approx \frac{\partial f_{F\text{-}P}}{\partial \ell} + \frac{\partial f_s}{\partial \ell} \qquad (II.17)$$

In summary; (1) The transition from the Boltzmann equation to equation (II.2) is acceptable only if the scattering cross-section $\sigma(\psi)$ falls off sufficiently rapidly with increasing ψ (faster than ψ^{-4}) beyond some small angle ψ_0. (2) Even then, any solution of equation (II.2) must be thought of as representing a smoothing of the true distribution function over path length intervals large compared to $\ell_0 = \frac{1}{4} D\psi_0$. Where the distribution function has already become smoothly-varying in phase space, this limitation is no longer important. However, as in the example we have analyzed the initial f is sharply peaked in phase space, the solution cannot be trusted until

an interval of time ℓ_0/v has elapsed. In any case, if $\sigma(\psi)$ is slowly varying in the interval $0<\psi<\psi_0$, changes in the distribution function over an interval $\Delta\ell<\ell_0$ can always be obtained from pure single scattering analysis. (3) If at some initial time the distribution function is essentially confined to a narrow region in phase space, its subsequent development within a larger domain of phase space, over an interval $\ell_0 \ll \ell \ll D$, is adequately approximated by regarding as a direct sum of the main solution and a contribution f_s coming from single, large angle scatterings;

$$f \approx f_{F\text{-}P} + f_s \qquad \text{(II.18)}$$

where f_s is to be included only for angles large compared to the mean angle for $f_{F\text{-}P}$. In the same problem analyzed above, the domain of validity of (II.18) corresponds to $0<\theta \ll \bar{\theta}^2/\psi_0$, the term being appended only for $\theta \gg \bar{\theta}$ and becoming important only beyond some critical angle, θ_c determined by setting $f_{F\text{-}P} \approx f_s$ and taking the root, if any, which lies well above $\bar{\theta}$. Finally a proper assessment of the errors involved in any approximation scheme for treating multiple scattering must depend on the details of the problem in question.

III.3.2 Applications to the Shallow Depth Problem

At the initial time, an electron is assumed to be located at the spatial origin $\vec{x}=0$ with velocity vector directed along the positive z axis. In the following treatment, we scale the distances by measuring them in units of D, the diffusion length. D is assumed to be independent of ℓ in the region under consideration. We start with studying the dependence on orientation of the velocity vector of the low spatial moments of f, in particular for times which are small compared to the diffusion time, i.e., for $\ell \ll 1$.

Consider first the zero-th spatial moment;

$$f_0(\theta,\ell) = \int f(\rho, z, \theta, \varphi, \ell)\, \rho\, d\rho dz \qquad (II.19)$$

which describes the distribution in velocity vector orientation, irrespective of spatial position. For this moment, after averaging over φ, equation (II.2) reduces to

$$\frac{\partial}{\partial\mu}(1-\mu^2)\frac{\partial f}{\partial\mu} = \frac{\partial f_0}{\partial \ell}, \qquad \mu \equiv \cos\theta \qquad (II.20)$$

and the solution consistent with the boundary condition is

$$f_0 = \frac{1}{4\pi}\sum_{m=0}^{\infty}(2m+1)\,P_m(\mu)\,e^{-m(m+1)\ell} \qquad (II.21)$$

where $P_m(\mu)$ is the Legendre polynomial.

In order to find out the rapidly convergent solution for $\ell \ll 1$, we exploit the integral representation of Legendre polynomial; i.e., for $\theta < \pi$,

$$P_m(\mu) = \frac{\sqrt{2}}{\pi}\int_\theta^\pi d\alpha \frac{\sin n\left[(m+\frac{1}{2})\alpha\right]}{(\cos\theta - \cos\alpha)^{1/2}} \qquad (II.22)$$

so that

$$4\pi f_o = \frac{1}{\sqrt{2}\pi}\int_\theta^\pi d\alpha \frac{\Sigma(\alpha)}{(\cos\theta - \cos\alpha)^{1/2}},$$

where

$$\Sigma(\alpha) = \sum_{m=-\infty}^{\infty} (2m+1)\sin\left[(m+\tfrac{1}{2})\alpha\right] e^{-m(m+1)\ell}.$$

With the Poisson sum formula, $\Sigma(\alpha)$ can be transformed into

$$\Sigma(\alpha) = \sum_{m=-\infty}^{\infty}\int_{-\infty}^{\infty} dx\, e^{-2\pi i m x}(2x+1)\sin\left[(x+\tfrac{1}{2})\alpha\right] e^{-x(x+1)\ell}$$

$$= -2\frac{\partial}{\partial\alpha}\sum_m (-1)^m \int_{-\infty}^{\infty} dx\, e^{-2\pi i m x}\cos\alpha x\, e^{-\ell x^2} e^{\ell/4}.$$

For sufficiently small ℓ, only the $m=0$ term need be retained in the above expression and we find

$$4\pi f_o \xrightarrow[\ell\to 0]{} \frac{1}{\sqrt{2\pi}}\frac{1}{\ell^{3/2}}\int_\theta^\pi d\alpha \frac{\alpha e^{-\alpha^2/4\ell}}{(\cos\theta - \cos\alpha)^{1/2}}.$$

We evalute this in the limit $\ell \to 0$ (but for arbitrary θ) and we get

$$f_0(\theta,\ell) \xrightarrow[\ell\to 0]{} \frac{1}{4\pi\ell}\left(\frac{\theta}{\sin\theta}\right)^{1/2} e^{-\theta^2/4\ell} \qquad (\text{II}.23)$$

which is consistent with the earlier result (II.3).

Now, to get information about average longitudinal displacement, we consider the higher moments of the distribution in the coordinate of spatial position, regarded as functions of the velocity vector orientation.

$$f_{(n;z)}(\theta,\ell) \equiv \int z^n f(\rho,z,\theta,\varphi,\ell)\,\rho\,d\rho\,dz \qquad (\text{II}.24)$$

Multiplying the equation (II.2) by z^n, integrating over all space, averaging over azimuth angle of velocity vector orientation, we find a set of coupled equations;

$$\frac{\partial f_{(n;z)}}{\partial \ell} - \frac{\partial}{\partial \mu}\left\{(1-\mu^2)\frac{\partial f_{(n;z)}}{\partial \mu}\right\} = \mu n f_{(n-1;z)} \qquad (\text{II}.25)$$

This is to be solved subject to the initial condition $f_{(n;z)}=0$ at $\ell=0$, provided $n>0$. It is evident that the solution for $f_{(n;z)}$, in terms of $f_{(n-1;z)}$, is given by

$$f_{(n;z)}(\theta,\ell) = \frac{n}{4\pi}\int_0^\ell d\ell' \sum_m (2m+1) P_m(\mu)\, e^{-m(m+1)(\ell-\ell')}$$

$$\times \int d\Omega' P_m(\mu') \mu' f_{(m-1;z)}(\theta', \ell') \qquad (II.26)$$

Since the zeroth moment f_o is already known, all of the higher moments can be obtained in succession. For example,

$$f_{(1;z)} = \frac{1}{8\pi} \sum_{m=0}^{\infty} P_m(\mu) \left\{ e^{-m(m-1)\ell} - e^{-(m+1)(m+2)\ell} \right\} \qquad (II.27)$$

Using the Poisson sum formula as before we find for the limit $\ell \to 0$ the result;

$$f_{(1;z)} \longrightarrow \ell \left(\frac{\sin\theta}{\theta} \right) f_o(\theta, \ell)$$

Now

$$\bar{z} = f_{(1;z)}(\theta, \ell) / f_o(\theta, \ell) \qquad (II.28)$$

is the average value of the z displacement at "time" ℓ for electrons whose velocity vector makes an angle θ with respect to the z axis; so we have

$$\bar{z} = \frac{\sum_{m=0}^{\infty} P_m(\mu) \left\{ e^{-m(m-1)\ell} - e^{-(m+1)(m+2)\ell} \right\}}{2 \sum_{m=0}^{\infty} (2m+1) P_m(\mu) e^{-m(m+1)\ell}} \qquad (II.29)$$

and

$$\bar{z}(\theta, \ell) \xrightarrow[\ell \to 0]{} \ell \left(\frac{\sin\theta}{\theta} \right).$$

We consider next the question of the lateral spread with time of a group of electrons all located initially at the origin, with the velocity vectors directed along the z axis. Define the moments

$$f_{(n;\rho)} = \int \rho^n f(\rho, z, \theta, \varphi, \ell)\, \rho\, d\rho\, dz \qquad (II.30)$$

The equation (II.2) then reduces to

$$\frac{\partial f_{(n;\rho)}}{\partial \ell} - \left\{ \frac{\partial}{\partial \mu}(1-\mu^2)\frac{\partial f_{(n;\rho)}}{\partial \mu} + \frac{1}{1-\mu^2}\frac{\partial^2 f_{(n;\rho)}}{\partial \varphi^2} \right\} = n \sin\theta \cos\varphi\, f_{(n-1;\rho)} \qquad (II.31)$$

which, for $n>0$, must be solved subject to $f_{(n;\rho)}=0$ as $\ell \to 0$. This has the solution

$$f_{(n;\rho)} = n \int_0^{\ell} d\ell' \sum_{\lambda=0}^{\infty} \sum_{m=-\lambda}^{\lambda} Y_{\lambda m}(\theta,\varphi)\, e^{-\lambda(\lambda+1)(\ell-\ell')} \times \int d\Omega'\, Y^*_{\lambda m}(\theta',\varphi') \sin\theta' \cos\varphi'\, f_{(n-1;\rho)}(\theta',\varphi',\ell') \qquad (II.32)$$

where the $Y_{\lambda m}$ are spherical harmonics. To determine the moment functions we proceed as before. With the given $f_0(\theta,\ell)$, we find

$$f_{(1;\rho)}(\theta,\varphi,\ell) = \frac{\cos\varphi}{8\pi} \frac{\partial}{\partial\theta} \sum_{m=1}^{\infty} \frac{1}{m} \left\{ P_{m-1}(\theta) - P_m(\theta) \right\}$$

$$\times \left\{ e^{-m(m-1)\ell} - e^{-m(m+1)\ell} \right\} \qquad (II.33)$$

Thus,

$$\bar{P}(\theta,\varphi,\ell) = \frac{f_{(1;P)}(\theta,\varphi,\ell)}{f_0(\theta,\ell)}$$

$$= \frac{\cos\varphi \frac{\partial}{\partial\theta} \sum_m \frac{1}{m} \left\{ P_{m-1}(\theta) - P_m(\theta) \right\} \left\{ e^{-m(m-1)\ell} - e^{-m(m+1)\ell} \right\}}{2 \sum_m (2m+1) P_m(\theta)\, e^{-m(m+1)\ell}}$$

$$(II.34)$$

To get the behavior of $\bar{P}$ for the limit, $\ell \to 0$, we work directly with the differential equation (II.31). We set

$$f_{(1;P)}(\theta,\varphi,\ell) = \bar{P}(\theta,\varphi,\ell) f_0(\theta,\ell) \qquad (II.35)$$

and insert this into equation (II.31) and, in the resulting equation for $\bar{P}$, retaining only the linear term in an expansion in power of ℓ. The result is given by;

$$\bar{P}(\theta,\varphi,\ell) \xrightarrow[\ell\to 0]{} \ell \cos\varphi \left(\frac{1-\cos\theta}{\theta} \right) \qquad (II.36)$$

the interpretation of this is the following. Let $\vec{\rho}$ be the projection on $X-y$ plane of the position vector $\vec{x}$; and let $\vec{v}_\rho$ be a unit vector directed along the projection of $\hat{v}$ in the $X-y$ plane. Then the average value of $\bar{P}$ is expressed by

$$\langle \bar{P} \rangle \xrightarrow[\ell\to 0]{} \ell \left(\frac{1-\cos\theta}{\theta} \right) \hat{v}_\rho \,. \qquad (II.37)$$

III.3.3 Diffusion In Deeper Regions

In the deeper region of a medium, the variation of elastic scattering cross-section with energy of electrons is no longer negligible due to the large number of inelastic collisions. To include the energy dependence of elastic scattering cross-section, we use ℓ as the parameter of energy of an electron instead of using inelastic scattering cross-section. The energy of an electron is assumed to be a well defined function of ℓ, i.e. we assume "continuous slowing down approximation" according to the linear stopping power. In the following treatment we retain the same boundary condition as before. To put the equation (II.1) in a more tractable form, we expand the angular density function in spherical harmonics;

$$f(\vec{x},\hat{v},\ell)=\sum_{m=0}^{\infty}\sum_{n=-m}^{m}\sqrt{\frac{(2m+1)}{4\pi}\frac{(m-n)!}{(m+n)!}}\,f_{mn}\,Y_{mn}(\theta,\varphi) \qquad (II.38)$$

and obtain from (II.1) and (II.38)

$$\frac{\partial f_{mn}}{\partial \ell}+\sum_{\lambda\mu}\vec{\nabla}f_{\lambda\mu}\cdot Q_{mn}^{\lambda\mu}$$
$$=n\sum_{\lambda\mu}f_{\lambda\mu}\iint Y_{mn}^{*}(\hat{v})\left[Y_{\lambda\mu}(\hat{v}')-Y_{\lambda\mu}(\hat{v})\right]$$
$$\times\,\sigma(\hat{v}\cdot\hat{v}',\ell)\,d\hat{v}\,d\hat{v}' \qquad (II.39)$$

where

$$Q_{mn}^{\lambda\mu} = \int Y_{mn}^{*}\,\hat{v}\,Y_{\lambda\mu}^{*}\,d\hat{v}$$

is a constant vector. The boundary conditions to be satisfied by f_{mn} are

$$f_{mn}(\vec{x},0) = \delta_{no}\delta(\vec{x})\,Y_{mn}(0) = \sqrt{\frac{2m+1}{4\pi}}\,\delta_{no}\delta(\vec{x}) \qquad (II.40)$$

With spherical harmonics expansion of angular density function, we easily recognize that the spatial distribution alone, regardless of the orientation of electrons, is $f_{oo}(\vec{x},t)$. The last integral in (II.39) can be carried out by expanding $\sigma(\hat{v}\cdot\hat{v}',t)$ in Legendre polynomials, using the addition theorem, orthogonality, and normalization of the spherical harmonics;

$$\frac{\partial f_{mn}}{\partial t} + K_m f_{mn} - \left(\frac{\partial}{\partial\rho} + \frac{n+1}{\rho}\right) f_{m+1,n+1} + (m-n+1)(m-n+2)\left(\frac{\partial}{\partial\rho} - \frac{n-1}{\rho}\right) f_{m+1,n-1}$$

$$+ \left(\frac{\partial}{\partial\rho} + \frac{n+1}{\rho}\right) f_{m+1,n-1} - (m+1)(m+n-1)\left(\frac{\partial}{\partial\rho} - \frac{n-1}{\rho}\right) f_{m-1,n-1}$$

$$- (m-n+1)\frac{\partial f_{m+1,n}}{\partial z} - (m+n)\frac{\partial f_{m-1,n}}{\partial z} = 0 \qquad (II.41)$$

where

$$K_m = 2\pi n \int_0^{\psi} \sigma(\psi)\left\{1 - P_m(\psi)\right\}\sin\psi\,d\psi \qquad (II.42)$$

Equation (II.41) are a set of coupled equations of infinite number. To obtain an approximate solution, we must truncate f_{mn}'s at a certain order. To estimate the error involved in this approximation, we again resort to the distribution of the orientation of velocity regardless of the spatial distribution. By integrating (II.41) over all space, and noting that the terms with $n \neq 0$ vanish because of the azimuthal symmetry of the problem, we get

$$\frac{\partial F_{mn}}{\partial \ell} + K_m F_{mn} = 0 \qquad \text{(II.43)}$$

where $F_{mn}(\ell) = \int f_{mo}(\vec{x}, \ell) d\vec{x}$. The solution to this equation is

$$F_m(\ell) = \sqrt{\frac{2m+1}{4\pi}} \exp\left(-\int_0^\ell K_m(\ell')\, d\ell'\right)$$

which satisfies the boundary conditions, so that

$$f_o(\vec{x}, \ell) = \int f(\vec{x}, \hat{v}, \ell)\, d\vec{x}$$

$$= \frac{1}{4\pi} \sum_{m=0}^{\infty} (2m+1) P_m(\mu) \exp\left(-\int_0^\ell K_m(\ell')\, d\ell'\right) \qquad \text{(II.44)}$$

which is basically consistent with equation (II.21). From (II.44) we find;

$$\langle P_m(\cos\theta) \rangle = \exp\left(-\int_0^\ell K_m(\ell')\, d\ell'\right) \qquad \text{(II.45)}$$

For a sharply-peaked distribution at small angle θ , we

can take

$$P_m(\cos\theta) \approx 1 - \frac{1}{4} m(m+1)\,\theta^2$$

so that

$$\int_0^{\ell} K_m(\ell')\,d\ell' \approx \frac{1}{4} m(m+1)\,\langle\theta^2\rangle$$

since the argument of the exponential in equation (II.45) is relatively small for high energies(>20 MeV) for small m. Therefore, to adequately approximate the relatively shallow depth region, we have to truncate the spherical harmonics expansion of the angular distribution function, at least, $m \sim 2/(\theta^2)^{1/2}$. For diffuse angular distribution, equation (II.44) obviously converges rapidly. In this case, truncating the spherical harmonics expansion at low would yield a good approximation. But, unlike the case of a peaked distribution, it is not easy to locate a point where this approximation becomes adequate. Thus, we arbitrarily take the point at which the average cosine of the polar angle becomes e^{-1}, that is,

$$\langle\cos\theta\rangle = \exp\left(-\int_0^{\ell} K_1\,d\ell'\right) \sim e^{-1}$$

or

$$\int_0^{\ell} K_1\,d\ell' = 1 = \int_{T_d(\ell_d)}^{T(0)} \frac{K_1\,dT}{|-dT/\rho\,d\ell|} \qquad \text{(II.46)}$$

where $(-dT/\rho\,d\ell)$ is the mass stopping power of a medium.

The average penetration depth of electrons can then be calculated from (II.46)by

$$\langle z_d \rangle = \int_0^{\ell_d} \langle \cos\theta(\ell') \rangle \, d\ell' \qquad (II.47)$$

We apply the Fourier-Bessel integral and Fourier transformation to (II.41) to find;

$$\frac{\partial g_{mn}}{\partial \ell} + K_m g_{mn} + k\left\{ g_{m+1,n+1} - g_{m-1,n+1} - (m+n+1)(m-n+2)\, g_{m+1,n-1} + (m+n)(m+n-1)\, g_{m-1,n-1} \right\} + i\omega\left\{ (m+n+1)\, g_{m+1,n} + (m+n)\, g_{m-1,n} \right\} = 0 \qquad (II.48)$$

with the boundary condition, $g_{mn}(k,\omega,0) = \frac{1}{2\sqrt{2\pi}}$ where

$$g_{mn}(k,\omega,\ell) = \frac{1}{\sqrt{2\pi}} \int_{-\infty}^{\infty} \int_0^{\infty} f_{mn}(P,z,\ell)\, e^{i\omega z} J_n(kP)\, P\, dP\, dz$$

In order to investigate the electron transport in the region where the depth is greater than the diffusion depth defined by (II.47), we retain only terms with both m and n up to 1. The solution $g_{00}(k,\omega,\ell)$, under this approximation is,

$$g_{00}(k,\omega,\ell) = \frac{1}{2\sqrt{2\pi}} \exp\left[-\left\{ \int_0^{\ell} \frac{d\ell'}{K_1(\ell')} \right\} (\omega^2 + bk^2) \right] \qquad (II.50)$$

The inverse transformation of (II.58) with normalization gives;

$$f_{\infty}(\rho,z,\ell)=\frac{1}{12\sqrt{\pi}\,X^{3/2}}\exp\left[-\frac{1}{24X}\left(\rho^2+6z^2\right)\right] \qquad (II.51)$$

where

$$X(\ell)=\int_0^{\ell}\frac{d\ell'}{K_1(\ell')} \qquad (II.52)$$

For the numerical calculation of spatial distribution in the depth region, we need the mass stopping power and the energy dependence of the scattering cross-section.(43) For simplicity, the Rutherford formula accounting for inelastic deflections is used. The "screening" effect of atomic electrons is known to be negligible for our application (43), and is omitted in our calculation. Thus,

$$2\pi n\,\sigma(\psi,\ell)=\frac{3}{4}(z+1)(N_A\Phi_0 z/A)(T+1)^2$$
$$\times\, T^{-2}(T+2)^{-2}(1-\cos\psi)^{-2} \qquad (II.53)$$

where

N_A is the Avogadro's number,

A is mass number,

$\Phi_0=8\pi e^4/3m^2c^4$,

and the functional relationship between T and ℓ is given as follows;

$$\ell(T) = \int_T^0 \frac{dT}{|-dT/\rho d\ell|} \quad (g cm^{-2}) \qquad (II.54)$$

where $(-dT/\rho d\ell)$ is the mass stopping power. Equation (II.54) hinges on the legitimacy of the "continuous slowing down approximation"(csda). In this approximation, the energy of an electron is supposed to be determined solely by the total track-length which the electron has travelled. A complete tabulation of mass stopping power and range data can be found in Berger and Seltzer.(44) Spencer considers the stopping power number B which is essentially a logarithmic function of the energy to be a constant. In this approximation the mass stopping power may be written as;

$$-\left(dT/\rho d\ell\right) = \frac{3}{4}\frac{N_A \Phi_0 Z}{A} B \left\{1-(T+1)^{-2}\right\}^{-1} \qquad (II.55)$$

from which follows the expression for (II.62)

$$\ell_0 - \ell(T) = (3N_A \Phi_0 Z B/4A)^{-1} T^2 (T+1)^{-1} \qquad (II.56)$$

Spencer also presented the function form of $K_m(\ell)$.

$$K_m(\ell) = \frac{3}{4}(Z+1)(N_A \Phi_0 Z/A) C_m \left\{\frac{(T+1)}{T^2}\right\}\left\{\frac{1}{[T^2/(T+1)]+4}\right\} \qquad (II.57)$$

where C_m's satisfy the following recurrence relations.

$$C_0 = 0$$

$$C_1 = -1$$

$$C_{m+1} = (2+m^{-1})C_m - (1+m^{-1})C_{m-1} - (2+m^{-1})$$

If, therefore, we define $\alpha = (3N_A\Phi_0 Z B/4\hat{A})^{-1}\cdot 4$, we may rewrite (II.56) in the form $T^2/(T+1) = [\ell_0 - \ell(T)]\cdot 4/\alpha$. Defining $d_m \equiv \frac{1}{4}(2+1)C_m/B$, it is easily seen that (II.57) may be represented with considerable accuracy by the form;

$$K_m(\ell) \approx \alpha d_m / [\ell_0 - \ell(T)][\ell_0 - \ell(T) + \alpha] \qquad (II.58)$$

The spatial distribution of electrons in the depth region then can be calculated from (II.51).

$$\int d\hat{v} f(\vec{x}, \hat{v}, \ell) = \int_0^{\ell_0} f_{00}(P, Z, \ell)\, d\ell$$

III.4 Discussion

Assuming that ℓ represents the estimate of the path-length of individual electrons, equation (II.21) means the orientations of the electrons are more random for larger ℓ or equivalently, lower energy electrons.(Figure 14) In this calculation, as electrons are assumed to be placed at the surface of a semi-infinite medium and oriented perpendicularly to the surface, it is likely that

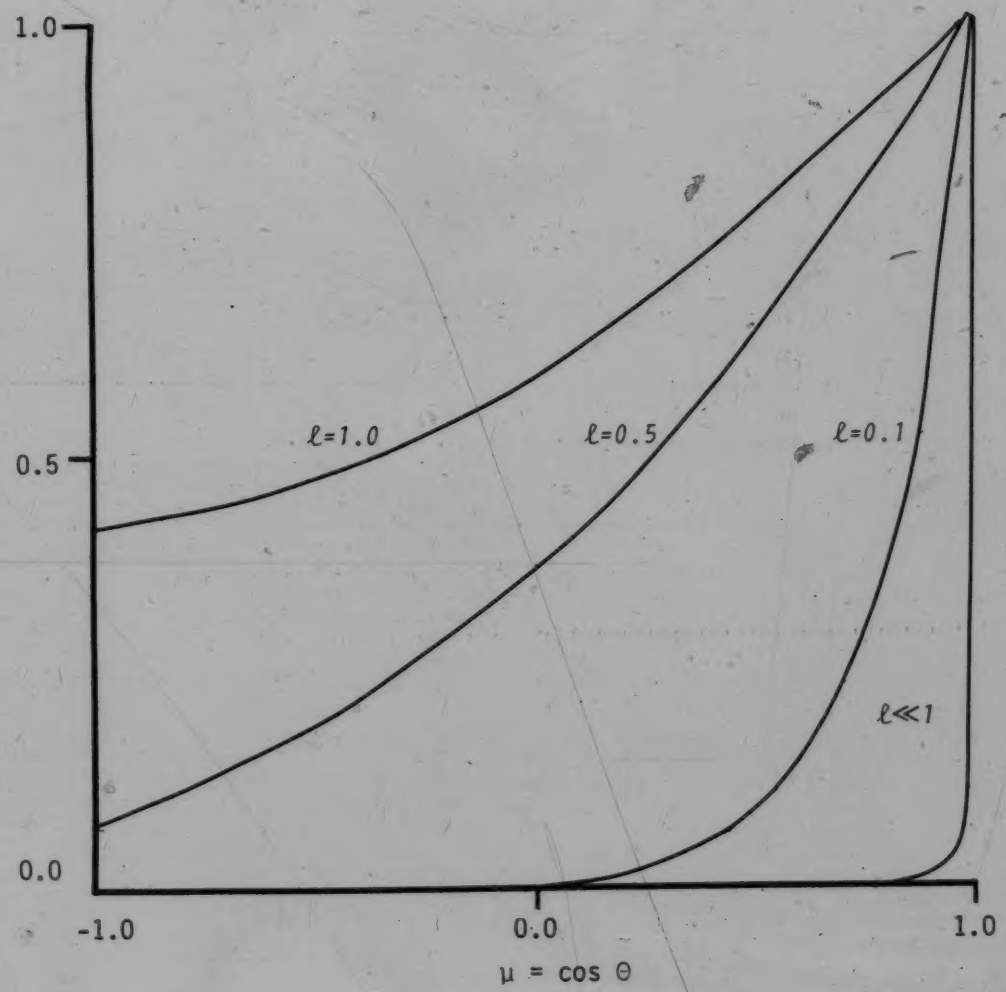

Fig. 14. The plot of the angular distribution function $f(\Theta,\ell)$ for various ℓ. $f(\Theta,\ell)$ is normalized to the $f(0,\ell)$. ℓ is the pathlength of an electron divided by the diffusion length.

most of electrons with large angle orientation are those which have relatively large ℓ . The contribution from a single large angle scattering to the number of electrons of large angle orientation would likely be significant after electrons has travelled for a long time "ℓ", because the single large angle scattering process is not a frequent event.

As for Fermi's model(46) of electron transport, since it incorporates the small angle approximation, it underestimates the probability that an electron has a large angle orientation(Figure 15). This is manifested in the expression (II.23). That is, the prediction obtained by Fermi equation differs from that obtained by the Boltzmann equation by as much as $(\sin\theta/\theta)^{1/2}$ even in the superficial region, $\ell \to 0$. This trend is expected to be more pronounced at the deeper region, due to the reason explained previously.

In addition to the inadequate description of angular distribution, Fermi's model is not appropriate for the description of spatial distribution of the incident electrons in the deeper region of semi-infinite medium because it does not include any delimiting parameter for the stopping of electrons. This is because this model is basically medium-oriented, that is, the primary objective of it is to get the distribution of electrons after they

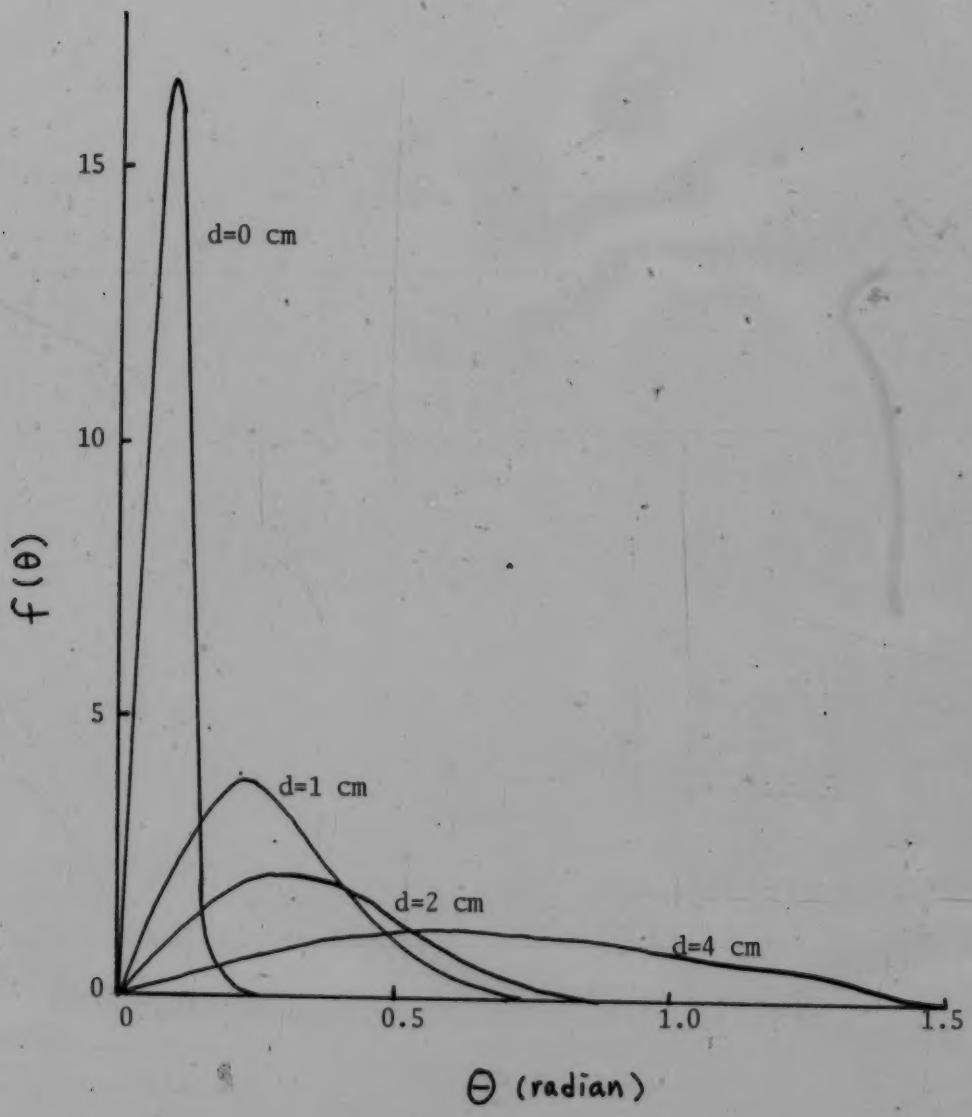

Fig. 15. The angular distribution of electrons. (56)

have been transported through a certain thickness of a slab. The distribution of electrons after they have lost a certain amount of their initial energy, is not considered and is more relevant to transport theory. The depth of a medium is not a suitable quantity to represent the physical state of individual electron because the fluctuation of energy loss and scattering spoils the relationship between the longitudinal position of electrons and their real physical state.

CHAPTER IV

CONCLUSION AND FUTURE WORK

The Boltzmann equation can be used to obtain the spatial fluence distribution of electrons which has immediate application to dose calculation in a complex medium. In addition, this equation provides the predictability of dose distribution without resorting to experimental parameters. Unfortunately, the complex nature of the Boltzmann equation seems to defy a solution in closed form, at least for a pencil beam boundary condition. However, with some reasonable approximations, the equation can be utilized to investigate some salient features of electron transport which would be useful for seeking numerical solutions, and designing future experiments.

Despite its potential impact on electron radiation therapy, the electron transport problem has been largely ignored. Several misinterpretations or incomplete interpretations of experimental results have originated

from this ignorance. For example, current understanding of the macroscopic effects of inhomogeneities is mainly related to the density of inhomogeneities. In fact, as described in the first chapter, because the microscopic elastic interactions between an incident electron and a constituent atom is influenced by the atomic number, the effect of inhomogeneities should be regarded as the combined action of the change of the density and the atomic number of the medium.

Regarding the atomic number effect of inhomogeneities, it is expected that the anisotropy of elastic scattering following the change of the atomic number would significantly contribute to the distortion of electron fluence distribution in a homogeneous medium, and thus affect the dose distribution. This contribution should be more significant while electrons are retaining higher energies, that is, at shallow depth of the medium. This is not only because the anisotropy of elastic scattering cross-section is more pronounced at higher energies, but also because at these higher energies, most of electrons are still well correlated spatially. Thus, the breadown in correlation would be more appreciable. This contribution should become less pronounced as the orientations of electrons become diffuse at deeper locations, because in this case, the anisotropy of scattering cross-section would not be as influential as

before in changing the electron fluence distribution. Even in a medium which is made up of the atoms whose scattering cross-sections are highly anisotropic, a point source particles would ultimately produce a spherically symmetric particle fluence distribution.

Better understanding of the electron transport problem can be utilized to a great advantage for innovation in the current dose administration technique. For example, medical linear accelerators which use magnetically scanned electron beams have some advantageous features, described in the first chapter, which cannot be found in the conventional accelerators using foil-scattering mechanism. However, to date, this magnet-scanning technique has only been regarded as one of the possible methods of producing broad beam without perception of other inherent advantages. It is conceivable that this technique would eliminate, in addition to the scattering foil, the necessity for;(a) field shaping devices, including the collimators, lead masks, and (b) external compensating materials for the effect of inhomogeneity. This technique can eliminate the former by choosing an appropriate scan pattern and the latter by modulating the intensity and/or energy of the each narrow beams. More standardization of a practical electron beam is also to be expected by using this technique.

It is certain that the essential ground work for the new generation of spot beam scanning technique(39), should be the development of transport theory for electrons. Even though the ultimate information we need is the dose distribution, the primary physical quantity to be sought in radiation physics should be the fluence of electrons. In this context, a new device for measuring the particle fluence with reasonable resolution is necessary to compliment the current dosimetric devices, and confirm theoretical expectations.

REFERENCES

1. BRASCH, A.,LANGE, F.: Aussichten and Moglichkeiten einer Therapie mit schnellen Kathidenstrahlen. Strahlentherapie 51:119-128, 1934

2. HASS, L.L., HARVEY, R.A., LAUGHLIN, J.S., BEATTIE, J.W., HENDERSON, W.J.: Medical Aspects of High Energy Electron Beams. Am. J. Roentgenol., Rad. Therapy & Nuclear Med. 72:250-259, 1954

3. OVADIA, J.,McALLISTER, J.: Dose distribution in grid Therapy with 15- to 33- MeV Electrons. Radiology 76:118-119, 1961

4. CARPENDER, J.W.J., SKAGGS, L.S., LANZL, L.H., GRIEM, M.L.: Radiation Treatment with High-Energy Electrons using Pencil Beam Scanning. Am. J. of Roentgen., Rad. Therap. and Nuc. Med. 90:221, 1963

5. TAPLEY, N.duV, FLETCHER, G.H.: Skin Reactions and Tissue Heterogeneity in Electron Beam Therapy. Part I.:clinical Experience. Radiology 84:812, 1965

6. LAUGHLIN, J.S.: High Energy Electron Treatment Planning for Inhomogeneities. Brit. J. Radiol. 38:143-147, 1965

7. HULTEN, G., SVENSSON, H.: Electron Depth Absorbed Doses for Small Phantom Depths. Acta. Radiol. Ther. Phys. Biol. 14:537, 1975

8. BRAHME, A.,SVENSSON, H.: Specification of Electron Beam Quality from the Central-Axis Depth Absorbed Dose Distribution. Med. Phys. 3:95, 1976

9. MUSTAFA, A.A.,JACKSON, D.F.:The Relation between X-ray CT Numbers and Charged Particle Stopping Powers and its Significance for Radiotherapy Treatment Planning. Phys. Med. Biol. 28:169-176, 1983

10. MILLAN, P.E.,MILLAN, S.,JERNANDEZ, A.,ANDREA, P.: Parametrization of Linear Accelerator Electron Beam for Computerized Dosimetry Calculations. Phys. Med. Biol. 24:827, 1979

11. PARKER, R.P.,HOBDAY, P.A.,CASSELL, K.J.: The Direct Use of CT Numbers in Radiotherapy Dosage Calculations for Inhomogeneous Media. Phys. Med. Biol.

24:802-809, 1979

12. LEACH, M.O.,WEBB, S.,BENTLEY, R.E.: A Rotate-Translate CT Scanner providing Cross-sectional Data suitable for Planning the Dosimetry of Radiotherapy Treatment. Med. Phys. 9:269, 1982

13. PFALZENER, P.M.,CLARKE, H.C.: Radiation Parameters of 6 to 20 MeV Scanning Electron Beams from the Saturne Linear Accelerator. Med. Phys. 9:117, 1982

14. MARBACH, J.R.,ALMOND, P.R.: Optimisation of Field Flatness and Depth Dose for Therapy Electron Beams. Phys. Med. Biol. 26:435-443, 1981

15. BRAHME, A.,HULTEN, G.,SVENSSON, H.: Electron Depth Absorbed Dose Distribution for a 10 MeV Clinical Microtron. Phys. Med. Biol. 20:39-46, 1975

16. de ALMEIDA, C.E.,ALMOND, P.R.: Comparison of Electron Beams from the Siemens Betatron and the Sagittaire Linear Accelerator. Radiology 111:439, 1974

17. ICRU REPORT 21(1972): Radiation Dosimetry: Electrons woth Initial Energies Between 1 and 50 MeV.

18. BERGER, M.J., SELTZER, S.M.: Calculation of Energy and Charge Deposition and of the Electron Flux in a Water Medium Bombarded with 20 MeV Electrons. Ann. New York Acad. Sci. 161:8, 1969

19. KESSARIS, N.D.:Penetration of High Energy Electron Beams in Water. Phys. Rev. 145:145, 1965

20. SEMPERT, M.,WIDEROE, R.: Untersuchungen uber Dosimetrie und Ausblendung von 30 MeV Elektronenstrahlen. Betron und Telekobalttherapie, Edited by Becker and Scheer. Springer Verlag, Berlin, pp. 182

21. ROSSI, B.B.: High Energy Particles. Prentice Hall, New York, 1956

22. SAUNDERS, J.E.,PETERS, V.G.: Backscattering from Metals in Superficial Therapy with High Energy Electrons. Brit. J. Radiol. 47:467, 1974

23. WEATHERBURN, H.,McMILLAN, K.T.P.,STEDEFORD, B.,DURRANT, K.R.: Physical Measurements and Clinical Observations on the Backscatter of 10 MeV Electrons from Lead Shielding. Brit. J. Radiol. 48:229, 1975

24. NUSSLIN, F.: Electron Backscattering from Lead in a Perspex Phantom. Brit. J. Radiol. 48:1041, 1975

25. BAILY, N.A.: Electron Backscattering. Med. Phys. 7:514, 1980

26. EKSTRAND, K.E.,DIXON, R.L.: The Problem of Obliquely Incident Beams in Electron Beam Treatment Planning. Med. Phys. 9:276, 1982

27. SIBATA, C.H.,de ALMEIDA, C.E.: Build-up Curves of Scanned High Energy Electron Beams from the Sagittaire Linear Accelerator. Med. Phys. 7:374, 1980

28. OVADIA, J.: Treatment Planning Consideration. In: Practical Aspects of electron Beam Treatment Planning, Edited by C.G. Orton and F. Bange, 1977, pp. 33.

29. SUNTHARALINGAM, N.: Dosimetry of Electron Beams. In: Practical Aspects of Electron Beam Treatment Planning, Edited by C.G. Orton and F. Bange, 1977, pp. 11.

30. BRAHME, A.,KRAEPELIEN, T.,SVENSSON, H.: Electron and Photon Beams from 50 MeV Racetrack Microtron. Acta. Radiol. Oncol. 19:305, 1980

31. BRAHME, A.,SVENSSON, H.: Radiation Beam Charactristics of a 22 MeV Microtron. Acta. Radilo. Oncol. 18:244, 1979

32. BRENNER, M.,KARJALAINEN, P.,RYTILA, A.,JUNGAR, H.: The Effect of Inhomogeneities on Dose Distributions of High Energy Electrons. Ann. New York Acad. Sci. 161:233, 1969

33. ALMOND, P.R.: Radiation Physics of Electron Beams. In: Clinical Applications of The Electron Beam. Edited by Tapley, N.duV., John Wiley & Sons, New York, 1976

34. LANZL, L.H: Electron Pencil Beam Scanning and its Application in Radiation Therapy. Front. Radiation. Ther. Onc. 2:55-66, 1968

35. HASS, L.L.,SANDBURG, G.H.: Modification of the Depth Dose Curves of Various Radiations by Interposed Bone. Brit. J. Radiol. 30:19-26, 1957

36. KAWACHI, K.: Calculation of Electron Dose Distribution for Radiotherapy Treatment Planning. Phys. Med. Biol. 20:571-577, 1975

37. GAGNON, W.F.,CUNDIFF, J.H.: Dose Enhancement from Backscattered Radiation at Tissue-Metal Interfaces irradiated with High Energy Electrons. Brit. J. Radiol. 53:466, 1980

38. HOGSTROM K.R.,MILLS, M.D.,ALMOND, P.R.: Electron Beam Dose Calculations. Phys. Med. Biol. 26:445, 1981

39. KANAI, T.,KAWACHI, K.,KUMAMOTO, Y.,OGAWA, H.,YAMADA, T.,MATSUZAWA, H.: Spot Scanning System for Proton Radiotherapy. Med. Phys. 7:365-369, 1980

40. BRAHME, A.,LAX, I.,ANDREO, P.: Electron Beam Dose Planning using Discrete Gaussian Beams.<Mathematical Background> Acta. Radiol. Onco. 20:147, 1981

41. LILLICRAP, S.C.,WILSON, P.,BOAG, J.W.: Dose Distributions In High Energy Electron Beams: Production of Broad Beam Distribution from Narrow Beam Data. Phys. Med. Biol. 20:30, 1975

42. CASE, K.M.,ZWEIFEL, P.F.: Linear Transport Theory. Addison Wesley, Mass., 1967

43. SPENCER, L.V.: Theory of Electron Penetration. Phys. Rev. 98:1597, 1955

44. BERGER, M.J.,SELTZER, S.M.: Tables of Energy Losses and Ranges of Electrons and Positrons. NASA SP-3012, National Aeronautics and Space Administration, washington, D.C., 1964

45. ATTIX, H.F.,FRANK, ROESCH, W.C.(ed.): Radiation Dosimetry(2nd ed.), Vol. 1, Fundamentals. Academy Press, New York and London, 1968

46. EYGES, L.: Multiple Scattering with Energy Loss. Phys. Rev. 74:1534, 1948

47. STERNICK, E.S.: Algorithms for Computerized Treatment Planning. In: Practical Aspects of Electron Beam Treatment Planning Edited by C.G. Orton and F. Bange, 1977, pp. 74.

48. HANSON, A.O.,LANZL, L.H.,LYMAN, E.M.,SCOTT, M.B: Measurement of Multiple Scattering of 15.7 MeV Electrons. Phys. Rev. 84:634, 1951

49. BATTISTA, J.J.: A Magnetic Spectrometer for Betatron Electrons. M.Sc. Thesis, University of Western Ontario, 1973

50. LAUGHLIN, J.S.,LUNDY, A.,PHILLIPS, R.,CHU, F.,SATTAR, A.: Electron Beam Treatment Planning in Inhomogeneous Tissue. Radiology 85:524-30, 1965

51. DAHLER, A.,BAKER, A.S.,LAUGHLIN, J.S.: Comprehensive Electron Beam Treatment Planning. Ann. N.Y. Acad. Sci. 161:193-213, 1969

52. BAGNE, F.: Electron Beam Treatment Planning System. Med. Phys. 3:31-38, 1976

53. PACYNIAK, J.M.,PAGNAMENTA, A.: Central Axis Percentage Depth Dose for High Energy Electrons. Rad. Res. 60:342-46, 1974

54. POHLIT, W.: Treatment Planning for Electron Beams in Inhomogeneous Media. Radiation Dosimetry, AAPM 1976 Summer School, PP 81-86

55. HOLT, J.G.,MOHAN, R.,CALEY, R.,BUFFA, A.,REID, A., SIMPSON, L.D.,LAUGHLIN, J.S.: Memorial Electron Beam AET Treatment Planning System. Procedings, "Practical Aspects of Electron Beam Treatment Planning ", Symposium, July 31, 1977 pp 70

56. HOGSTROM, K.R.: Dosimetry of Electron Heterogeneities. Preprint, University of Texas

APPENDIX A

RELATIONSHIP OF BOLTZMANN AND FERMI EQUATIONS

As a first step in deriving the Fermi equation from the linearized Boltzmann equation (II.1), we have to modify the equation (II.1) slightly, because there are substantial differences between the two models, notably;

(a) In Fermi's model, electrons remains on a plane containing the initial trajectory after scattering, that is, scattering process changes only the polar angle of the orientation of the incident electron.

(b) As the energy losses of electrons are ignored in Fermi's model, the path-length of an electron, ℓ, is not considered.

(c) Fermi's model defines a probability that an electron traversing the thickness Δt of a scattering medium will be deflected by an angle $(\theta, d\theta)$ regardless of the detailed multiple scattering processes.

Due to this particular treatment of multiple scattering, the necessary changes of the equation (II.1) for the comparison are;

(a) There is no φ -dependence in σ and f . In addition, the scattering cross-section becomes a function of

$$\psi = \cos^{-1}(\hat{v}\cdot\hat{v}') = \theta' - \theta$$

With these changes the equation (II.1) reads;

$$\hat{v}\cdot\vec{\nabla} f(\vec{x},\theta) = n\int d\theta' \left[f(\vec{x},\theta') - f(\vec{x},\theta) \right] \sigma(\theta'-\theta) \qquad (A.1)$$

(b) The ℓ -dependence of the angular distribution function, f , and the scattering cross-section, σ , in the equation (II.1) should be ignored.

As $\sigma(\theta'-\theta)$ is peaked at very small $(\theta'-\theta)$, we expand $f(\vec{x},\theta')$ in a Taylor series of $(\theta'-\theta)$.

$$f(\vec{x},\theta') \approx f(\vec{x},\theta) + (\theta'-\theta)\frac{\partial f}{\partial \theta} + \frac{(\theta'-\theta)^2}{2!}\frac{\partial^2 f}{\partial \theta^2}$$

Thus, the right hand side of (A.1) becomes;

$$n\left[\left\{ \int_{-\infty}^{\infty} d\theta' (\theta'-\theta)\sigma(\theta'-\theta) \right\} \frac{\partial f}{\partial \theta} + \left\{ \int_{-\infty}^{\infty} d\theta' (\theta'-\theta)^2 \sigma(\theta'-\theta) \frac{\partial^2 f}{\partial \theta^2} \right\} \right] .$$

The limit of integration can be extended

from $-\infty$ to ∞ , since $\sigma(\theta'-\theta)$ is very sharply peaked at $\theta' = \theta$. Since $\sigma(\theta'-\theta)$ is even in $(\theta'-\theta)$, the equation (A.1) reduces to;

$$\sin\theta \frac{\partial f}{\partial \rho} + \cos\theta \frac{\partial f}{\partial z} = \left[n \int_{-\infty}^{\infty} d\theta' \, \sigma(\theta'-\theta)(\theta'-\theta)^2 \right] \frac{\partial^2 f}{\partial \theta^2} \quad (A.2)$$

According to the Fermi's treatment of angular deflection, explained in (c), the expression in the bracket of the equation (A.2) is equivalent to $1/\omega^2$. Finally, since θ is small, (A.2) reduces to Fermi equation.(49)

$$\frac{\partial f}{\partial z} = -\theta \frac{\partial f}{\partial \rho} + \frac{1}{\omega^2} \frac{\partial^2 f}{\partial \theta^2}$$

Q.E.D.